

Tessellated Wasserstein Auto-Encoders

Kuo Gai^{1,2} and Shihua Zhang^{1,2,*}

¹*Academy of Mathematics and Systems Science*

Chinese Academy of Sciences

Beijing 100190, China

²*School of Mathematical Sciences*

University of Chinese Academy of Sciences

Beijing 100049, China

*Email: zsh@amss.ac.cn

Abstract

Non-adversarial generative models are relatively easy to train and have less mode collapse compared to adversarial ones. However, they are not very accurate in approximating the target distribution in the latent space because they don't have a discriminator. To this end, we develop a novel non-adversarial framework called Tessellated Wasserstein Auto-Encoders (TWAE) to tessellate the support of the target distribution into a given number of regions by the centroidal Voronoi tessellation (CVT) technique and design batches of data according to the tessellation instead of random shuffling for accurate computation of discrepancy. Theoretically, we demonstrate that the error of estimate to the discrepancy decreases when the numbers of samples n and regions m of the tessellation become larger with rates of $\mathcal{O}(\frac{1}{\sqrt{n}})$ and $\mathcal{O}(\frac{1}{\sqrt{m}})$, respectively. Given fixed n and m , a necessary condition for the upper bound of measurement error to be minimized is that the tessellation is the one determined by CVT. TWAE is very flexible to different non-adversarial metrics and can substantially enhance their generative performance in terms of Fréchet inception distance (FID) compared to existing ones. Moreover, numerical results indeed demonstrate that TWAE is competitive to the adversarial model, demonstrating its powerful generative ability.

Keywords: Non-adversarial generative models, centroidal Voronoi tessellation, sphere packing, optimal transport, optimization with non-identical batches

1. Introduction

Knowing the distribution of data is a fundamental task of data science. Prior distributions such as Laplacian, Gaussian and Gaussian mixture distributions are often used to model the data. However, their ability of representation is limited. With the rise of deep learning, we can use more parameters to model the distribution accurately. The basic assumption of such methods is that complex high-dimensional data such as images concentrate near a low-dimensional manifold. Generative adversarial network (GAN) [17] and Wasserstein auto-encoder with generative adversarial network (WAE-GAN) (also known as adversarial auto-encoder (AAE)) [36; 43] are the representatives and have many variants. GAN trains a generator to generate new samples and a discriminator to teach the generator to improve its quality. From a probabilistic view, the generator maps points from a simple

low-dimensional distribution such as a uniform distribution or a Gaussian distribution to the target high-dimensional distribution (e.g., face or handwriting images), while the discriminator computes the discrepancy between the generated distribution and the target one. WAE-GAN trains an invertible mapping between two distributions with the Wasserstein distance as the reconstruction loss, i.e., an encoder from the data space to the latent space and a decoder from the latent space to the data space. WAE-GAN employs GAN to minimize the discrepancy between the output of the encoder and the samplable prior distribution in the latent space. Both methods use adversarial training, i.e., a two player game between generator (encoder) and discriminator.

As we know that GAN is hard to train. Arjovsky et al. [2]; Arjovsky and Bottou [1] ascribed this to the choice of discrepancy. Classifical GAN uses KL-divergence and performs good under some tricks [41]. But in theory, when the supports of two distributions are disjoint, KL-divergence fails and causes unstability of the model. A more stable variant Wasserstein-GAN (WGAN) introduced from the optimal transport view uses a discriminator with clipped parameters to compute the Wasserstein distance. However, clipping limits the discriminator to find the subtle difference between two distributions. Another strategy imposes the one-Lipschitz constraint by regularization methods. Since the Wasserstein distance is a real distance, the optimization appears more stable and converges faster than GAN. Apart from the optimal transport, several other studies have also been proposed to explain and improve this [41; 37; 20].

The complexity of high-dimensional data and the instability of adversarial models lead to mode collapse, which is the main obstacle for GANs in many applications. The mode collapse in GANs refers to the problem of overfitting to a part of the training modes and forget the rest. Lucic et al. [34] showed that even the best GAN dropped 72% of the modes. In theory, Arora et al. [3] proved that the trained distribution can not converge to the target one with several standard metrics. This can be blamed on the adversarial mechanism. In game theory, based on gradient descent optimization algorithm, the discriminator and generator find a local Nash equilibrium rather than a global one. From a statistical view, the discriminator has cumulative preference of mode when it classifies real and fake data in the training process, since the discriminator is trained based on the former step. So the discriminator is sensitive to some modes and insensitive to others. More formally, the estimation of discrepancy is biased, which makes the generated distribution not converge to the target one.

To solve this problem, a potential approach is to find alternatives of the adversarial mechanism by computing the discrepancy without neural network for discrimination. For example, a kernel-based method maximum mean discrepancy (MMD) shows a good property on approximating the independent and identically distributed (i.i.d.) Gaussian distribution and finds its usage on WAE-MMD [43] and MMD-GAN [30]. However, MMD only matches principle features of two distributions and lose other ones which cannot be captured by the kernel. As to the discrepancy of arbitrary distributions, researchers have introduced a new metric called the sliced-Wasserstein (SW) distance [5], which has similar qualitative properties with the Wasserstein distance. But it is much easier to compute. Inspired by the one-dimensional case of the Wasserstein distance, the data is projected onto an one-dimensional subspace for analytical solution, then the SW distance is obtained by integrating over all the subspaces. Thus, the number of samples needed to estimate the

integration increases as the dimension of data goes up. More generally, the SW distance has been generalized to the high-dimensional situation, where the data is projected into a k -dimensional subspace ($k \geq 2$), which maximizes their transport cost [40; 32]. This distance is more robust to noise compared with the Wasserstein distance because of its dimension reduction operation.

Compared to adversarial training, non-adversarial approaches have no cumulative preference since they do not memorize historical information and are easy to train due to the unemployment of the discriminator. However, since the distribution of high-dimensional data concentrates near a low-dimensional manifold, where the Euclidean distance is no longer effective, non-adversarial approaches are not over-parameterized to learn the distance on the manifold. So they may be cursed by high dimensionality. This means, when the dimension is high and the shape of the manifold is complicated, the error of the estimation to the discrepancy may be beyond tolerance. As a consequence, the performance of non-adversarial algorithms such as variational auto-encoder (VAE) [24], WAE-MMD, sliced-Wasserstein auto-encoder (SWAE) [25] are not as good as that of WAE-GAN or variants of GAN under similar architectures of neural network.

In this paper, we develop a novel non-adversarial framework—Tessellated Wasserstein Auto-Encoders (TWAE) to tessellate the support of the target distribution in the latent space into a given number of regions and design batches of data according to the tessellation instead of random shuffling. In more detail, the cost function of classical generative auto-encoders consists of the reconstruction error in the data space and the discrepancy error in the latent space. To compute the latter, TWAE separates the computation of the global discrepancy into some local ones. To do this, we need to obtain a tessellation of the support of both the target and generated distributions (Fig. 1). We implement this task in two steps: first we tessellate the support of the prior distribution; second we cluster the encoded data corresponding to the tessellation. For the first step, we provide two ways to achieve the tessellation: centroidal Voronoi tessellation (CVT) and sphere packing. CVT can generate points which are the centroids of the corresponding Voronoi regions. Asymptotically speaking, all regions of the optimal CVT are congruent to a basic region. CVT can be applied to a connected set in R^n with arbitrary shapes. The sphere packing approach can tessellate the space into exactly congruent regions with E_8 -lattice in R^8 and Leech lattice in R^{24} . For the second step, we adopt an assignment algorithm to keep the correspondence of the encoded data and the regions of tessellation. Thereby the discrepancy on the whole support is separated into a sum of local discrepancies on each region. Compared with traditional ways of sampling on the whole support, TWAE can sample specially in each region. As a result, we can force the generated distribution to approximate the target one better. Since the tessellation is independent of discrepancy metrics, TWAE is compatible to different ones and enhance their performance.

The rest of this paper is organized as follows. In section 2, we start from the optimal transport and briefly review the optimal transport-based generative methods. To the end, we introduce CVT and sphere packing as basic tools to achieve the tessellation. In section 3, we describe TWAE in details. In section 4, we derive the sample and measurement error of TWAE theoretically. In section 5, we conduct extensive experiments to demonstrate the effectiveness of TWAE. In section 6, we provide discussion and conclusion.

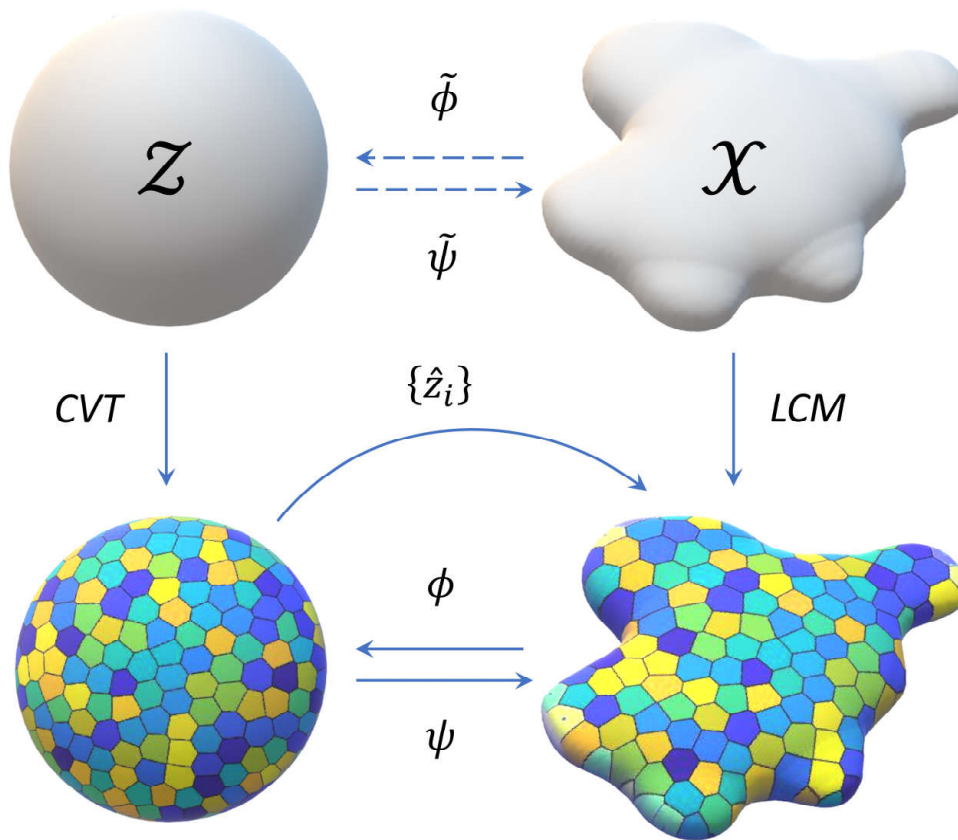


Figure 1: Illustration of TWAE. In a traditional way, the encoder $\tilde{\phi} : \mathcal{X} \rightarrow \mathcal{Z}$ and decoder $\tilde{\psi} : \mathcal{Z} \rightarrow \mathcal{X}$ are trained using randomly shuffled batches of data. In TWAE, the support of a known distribution is tessellated by the centroidal Voronoi tessellation (CVT) procedure, then the batch of data is designed with the least cost method (LCM) by their distance to the centroid $\{\hat{z}_i\}$ of each region. In the end, the auto-encoder (ϕ, ψ) is trained over region by region.

2. Related Work

In this section, we start from the optimal transport in Sec 2.1 and briefly review the optimal transport-based generative methods such as WGAN [2], sliced-Wasserstein GAN (SWGAN) [9], WAE and SWAE [25] in Sec 2.2. We further introduce CVT and sphere packing as basic tools to achieve the tessellation in Sec 2.3 and 2.4 respectively.

2.1 Optimal transport

The optimal transport problem stems from a problem on transporting commodities. Suppose there are m sources x_1, \dots, x_m for a commodity, with a_i units of supply at x_i and n sinks y_1, \dots, y_n for it, with b_j units of demand at y_j , c_{ij} ($i = 1, \dots, m; j = 1, \dots, n$) is the cost of transporting one unit of this commodity from x_i to y_j . We wish to find a

transport plan $\{f_{ij} | i = 1, \dots, m; j = 1, \dots, n\}$ to minimize the total cost. The problem can be formulated as

$$\begin{aligned} \min \quad & \sum_{i,j} c_{ij} f_{ij} \\ \text{s.t.} \quad & \sum_{j=1}^n f_{ij} = a_i, \quad i = 1, \dots, m \\ & \sum_{i=1}^m f_{ij} = b_j, \quad i = 1, \dots, n \\ & f_{ij} \geq 0, \end{aligned} \tag{1}$$

which can be solved by linear programming. Since the computational complexity of solving (1) is $\max\{m^3, n^3\}$, it can be expensive when $\max\{m, n\}$ is large. One solution for this computational problem is by using the entropic regularized version of optimal transport [8]. It can trade off a little optimality in exchange for an improved complexity of $\mathcal{O}(\max\{m^2, n^2\}/\epsilon^2)$, where $\epsilon > 0$ stands for the accuracy level [13; 31], which is more scalable than solving (1) by using linear programming. However, it is still expensive when we need to compute the optimal transport problem repeatedly, especially in learning the data distribution.

With the development of measure theory, the optimal transport problem can be stated as follows

$$W_c(P_x, P_y) = \inf_{\mathcal{T}} \mathbb{E}_{x \sim P_x} [c(x, \mathcal{T}(x))], \tag{2}$$

where $\mathcal{T} : X \rightarrow Y$ is a measure preserving transformation. This is known as the Monge formulation of the optimal transport problem [44]. There can be no admissible \mathcal{T} , for instance if P_x is a Dirac delta and P_y is not. To overcome this difficulty, Kantorovich [23] proposed the following way to relax this problem

$$W_c(P_x, P_y) = \inf_{\Gamma \in \Pi(P_x, P_y)} \mathbb{E}_{(x,y) \sim \Gamma} [c(x, y)], \tag{3}$$

where $\Pi(P_x, P_y)$ denotes the set of all joint distributions $\Gamma(x, y)$ whose marginals are respectively P_x and P_y . $c : X \times Y \rightarrow [0, \infty]$ is the cost function of transport. Particularly, W_1 and W_2 denote the Wasserstein distance when $c(x, y) = \|x - y\|_1$ and $c(x, y) = \|x - y\|_2^2$, respectively. Intuitively, $\Gamma(x, y)$ indicates how much “mass” must be transported from x to y in order to transform the distribution P_x into the distribution P_y . The infimum of the transport cost is called the Wasserstein distance of two distributions P_x and P_y . The Wasserstein distance is a true distance and has a finer topology to guarantee convergence when minimize the distance. But the Wasserstein distance is hard to compute because the feasible region of $\Pi(P_x, P_y)$ is too large to search. If the two distributions are assumed to be Gaussian, i.e., $x \sim \mathcal{N}(m_1, \Sigma_1)$, $y \sim \mathcal{N}(m_2, \Sigma_2)$ with the means $m_1, m_2 \in \mathbb{R}^p$ and the covariance $\Sigma_1, \Sigma_2 \in \mathbb{R}^{p \times p}$, their squared Wasserstein distance has a closed form [39]

$$GW^2 = W_2^2(P_x, P_y) = \|m_1 - m_2\|_2^2 + \text{tr} \left(\Sigma_1 + \Sigma_2 - 2 \left(\Sigma_2^{1/2} \Sigma_1 \Sigma_2^{1/2} \right)^{1/2} \right). \tag{4}$$

This is denoted as the GW distance.

2.2 Limit laws of the empirical Wasserstein distance

In practice, the size of data set $\{x_i\}_{i=1}^N$ is too large for the linear programming in (1) and we sample batches for better computation. Let P_N denote the empirical distribution of $\{x_i\}_{i=1}^N$, and P_n denote the empirical distribution of n i.i.d. samples from P_N . Thus, the speed of convergence of the Wasserstein distance P_n to P_N is of importance. Sommerfeld and Munk [42] showed that the convergence rate is $n^{-\frac{1}{2}}$, i.e.,

Theorem 1 *With n approaching infinity*

$$\sqrt{n}W_2^2(P_n, P_N) \rightarrow \gamma_1,$$

where γ_1 is a random variable correlated with P_N .

This theorem indicates that the convergence rate of empirical distribution is independent of the dimension. So we need not worry about the curse of dimensionality. However, if P is absolutely continuous on R^d , then $\mathbb{E}[W_2(P_n, P)] > Cn^{-\frac{1}{d}}$ [46]. Since computation of the GW distance is based on mean and covariance of empirical distributions, this asymptotic property can be generalized to the GW distance.

Theorem 2 *Let $P \neq Q$ be Gaussian, $P \sim N(m_1, \Sigma_1)$, $Q \sim N(m_2, \Sigma_2)$ with Σ_1 and Σ_2 having full rank. Let P_n and Q_n be generated by i.i.d. samples $z_1, \dots, z_n \sim Q$ and $\tilde{z}_1, \dots, \tilde{z}_n \sim P$, respectively. P'_n is an independent copy of P_n . Then with n approaching infinity*

$$\begin{aligned} \sqrt{n}(GW^2(P_n, Q_n) - GW^2(P, Q)) &\rightarrow N(0, w), \\ nGW^2(P_n, P'_n) &\rightarrow \gamma_2, \end{aligned}$$

where w is correlated with P and Q , and γ_2 is correlated with P .

When the dimension of distributions is one, similar results hold for continuous distributions under moderate conditions [4].

Theorem 3 *Let P, Q be continuous distributions on \mathbb{R} . Let P_n and Q_n be generated by i.i.d. samples $z_1, \dots, z_n \sim Q$ and $\tilde{z}_1, \dots, \tilde{z}_n \sim P$ respectively. P'_n is an independent copy of P_n . Let*

$$J_2(P) = \int_{F^{-1}(0)}^{F^{-1}(1)} \frac{F(x)(1-F(x))}{p(x)} dx, \quad (5)$$

where p is the density of distribution P and F is the cumulative function of P . If $\max\{J_2(P), J_2(Q)\} < \infty$, then with n approaching infinity

$$\begin{aligned} \sqrt{n}(W_2^2(P_n, Q_n) - W_2^2(P, Q)) &\rightarrow N(0, \sigma^2), \\ nW_2^2(P_n, P'_n) &\rightarrow \gamma_3, \end{aligned}$$

where σ^2 is the variance correlated with P and Q , and γ_3 is a random variable correlated with P .

2.3 Optimal transport-based generative models

Arjovsky et al. [2] first approached the problem of generative modeling from the optimal transport view. The infimum in (2) is highly intractable. On the other hand, when $c(x, y) = \|x - y\|_1$, the Kantorovich-Rubinstein duality [45] tells us that

$$\begin{aligned} W_1(P_x, P_y) &= \inf_{\Gamma \in \Pi(P_x, P_y)} \mathbb{E}_{(x, y) \sim \Gamma} [\|x - y\|_1] \\ &= \sup_{\|f\|_L \leq 1} (\mathbb{E}_{x \sim P_x} [f(x)] - \mathbb{E}_{y \sim P_y} [f(y)]), \end{aligned} \quad (6)$$

where the supremum is over all the one-Lipschitz functions $\{f : \mathcal{X} \rightarrow \mathbb{R}\}$. The function f is approximated by a parameterized family of functions $\{f_w\}_{w \in \mathcal{W}}$, where \mathcal{W} is the parameter space. Arjovsky et al. [2] suggested to impose the one-Lipschitz constraint to force parameters w lie in a compact space by clipping the weights to a fixed box. Gulrajani et al. [18] introduced a soft version of the constraint with a penalty on the gradient norm for random samples by optimizing

$$L = \mathbb{E}_{x \sim P_x} [f(x)] - \mathbb{E}_{y \sim P_y} [f(y)] + \lambda \mathbb{E}_{\hat{x} \sim P_{\hat{x}}} [(\|\nabla_{\hat{x}} f(\hat{x})\|_2 - 1)^2]. \quad (7)$$

To improve the stability of WGAN, Deshpande et al. [9] developed a mechanism based on random projections as an alternative to the black-box discriminator. Notice that the squared Wasserstein distance of two one-dimensional distributions P_x and P_y can be estimated accurately by sorting their samples. Suppose x_i, y_i ($i = 1, \dots, N$) are independently sampled from P_x and P_y , and $x_i \leq x_{i+1}, y_i \leq y_{i+1}$ for all $i \in \{1, \dots, N - 1\}$, then

$$W_2^2(P_x, P_y) = \inf_{\Gamma \in \Pi(P_x, P_y)} \mathbb{E}_{(x, y) \sim \Gamma} [\|x - y\|_2^2] \approx \frac{1}{N} \sum_{i=1}^N (x_i - y_i)^2. \quad (8)$$

Generally, if P_x and P_y are d -dimensional distributions, we project the sampled d -dimensional points onto one-dimensional spaces spanned by directions w and integrate over all possible directions w on the unit sphere S^{d-1} . Then we obtain the SW distance

$$SW_2^2(P_x, P_y) = \int_{w \in S^{d-1}} W_2^2(P_{x|w}, P_{y|w}) dw. \quad (9)$$

Hereby $P_{x|w}$ and $P_{y|w}$ denote the projected distributions on the subspace spanned by w . The SW distance is a real distance and is equivalent to the Wasserstein distance as the following property holds [5]

$$SW_2^2(P_x, P_y) \leq C_d W_2^2(P_x, P_y) \leq C_d R^{\frac{1}{d+1}} SW_2^{\frac{1}{d+1}}(P_x, P_y), \quad (10)$$

where $C_d > 0$ is a constant correlated with the dimension d , and $P_x, P_y \in \mathcal{P}(B(0, R))$, where $B(0, R)$ is the ball with radius R and the origin as the center point, $\mathcal{P}(\cdot)$ is the space of probability measure. The SW distance can be regarded as a good alternative to the Wasserstein distance because it can be easily acquired by random projections. However, since the area of a sphere with a radius of r in \mathbb{R}^d is proportional to r^{d-1} , the number of projections goes up exponentially with the dimension of data. Hence, the huge computation

caused by the curse of dimensionality becomes a main obstacle to put it into practice. The SW-based methods sacrifice accuracy to the discrepancy for the privilege of stability without the discriminator.

Alternatively, Deshpande et al. [10] proposed the max sliced-Wasserstein distance (Max-SW) to distinguish the probability distribution using only one important direction. Even though its performance in GANs is better than the SW distance, it can miss some important differences between two distributions in high-dimensional space. Nguyen et al. [38] proposed distributional sliced-Wasserstein distance (DSW) to search for an optimal distribution of important directions. The DSW distance has much better performance than the SW distance for GANs while has similar computational time as the SW distance. Kolouri et al. [26] proposed the generalized sliced-Wasserstein distance (GSW) to replace the linear projections in the SW distance with non-linear projections, which can fit the manifold of data better. They also suggested to generalize the Max-SW distance to the Max-GSW distance by using a single projection as long as it leads to a space with the maximal distance. With a neural network as the non-linear projection function, minimizing Max-GSW between two distributions is analogical to adversarial learning, where the goal of the adversarial network is to distinguish the two distributions. One can also solve the optimal transport problem in generative models through solving the Monge-Ampère equation. This equation can be linearized to the McKean-Vlasov equation and numerically solved using the forward Euler iteration [15]. Furthermore, Lei et al. [28] proposed a variational approach named AE-OT to solve the discrete Monge-Ampère equation explicitly. AE-OT separates the computation of OT from the training of neural network and improves the transparency of generative models.

Another main stream of generative models is based on auto-encoders. Different from GANs, generative auto-encoders approximate a prior distribution in the latent space. Their generalized formulation is as follows

$$\min_{\phi, \psi} \mathbb{E}_{x \sim P_x} [c(x, \psi(\phi(x)))] + \lambda D(P_z || Q_z), \quad (11)$$

where ϕ is the encoder, ψ is the decoder, P_x is the data distribution, P_z is a prior samplable distribution, Q_z is the empirical distribution of the encoded data $z = \phi(x)$, and λ indicates the relative importance of the discrepancy. In WAE [43], GAN and MMD have been proposed (denoted as WAE-GAN and WAE-MMD respectively). In SWAE [25], the choice of D in (11) is the SW distance.

2.4 Centroidal Voronoi Tessellation

Given an open set $\Omega \subseteq \mathbb{R}^d$, the set $\{V_i\}_{i=1}^k$ is called a tessellation of Ω if $V_i \cap V_j = \emptyset$ for $i \neq j$ and $\cup_{i=1}^k \bar{V}_i = \bar{\Omega}$ ($\bar{\Omega}$ means the closed hull of set Ω). Given a set of points $\{\hat{z}_i\}_{i=1}^k$ belonging to $\bar{\Omega}$, the set $\{\hat{V}_i\}_{i=1}^k$ is called a Voronoi tessellation if the Voronoi region \hat{V}_i corresponding to the point \hat{z}_i is defined by

$$\hat{V}_i = \{x \in \Omega \mid \|x - \hat{z}_i\| < \|x - \hat{z}_j\| \text{ for } j = 1, \dots, k, j \neq i\}. \quad (12)$$

The points $\{\hat{z}_i\}_{i=1}^k$ are called generators. In the rest of this paper, without special mention, a generator denotes the generator of tessellation rather than that of GAN. Given a region

$V \subseteq \mathbb{R}^d$ and a density function ρ , the mass centroid z^* of V is defined by

$$z^* = \frac{\int_V y \rho(y) dy}{\int_V \rho(y) dy}. \quad (13)$$

If $\hat{z}_i = z_i^*$, $i = 1, \dots, k$, i.e., the mass centroid of the region is exactly the generator, we call such a tessellation a CVT [12].

Next, we introduce the classical Lloyd's method to construct an approximate CVT in the following steps: **Step 0**: Select an initial set of k points $\{z_i\}_{i=1}^k$ using a sampling strategy (e.g., Monte Carlo sampling); **Step 1**: Construct the Voronoi tessellation $\{V_i\}_{i=1}^k$ of Ω associated with the points $\{z_i\}_{i=1}^k$; **Step 2**: Compute the mass centroids of the Voronoi regions $\{V_i\}_{i=1}^k$ found in **Step 1**; these centroids are the new set of points $\{z_i\}_{i=1}^k$; **Step 3**: If this new set of points meets some convergence criteria, then terminate; otherwise, return to **Step 1**. The Lloyd's method can be viewed as an alternative iteration between the Voronoi tessellation construction and centroid computation. Clearly, a CVT is a fixed point of the iteration. If we define a clustering energy by

$$\mathbb{K}(\{\hat{z}_i\}_{i=1}^k, \{\hat{V}_i\}_{i=1}^k) = \sum_{i=1}^k \int_{\hat{V}_i} \rho(y) \|y - \hat{z}_i\|^2 dy, \quad (14)$$

then the energy associated with the Voronoi tessellation decreases monotonically during the Lloyd iterations until a CVT is reached [12]. Apart from the Lloyd method, there is another simple one called K-means method (also known as probabilistic Lloyd method), which relies very little on the geometric information. The K-means method is defined as follows: **Step 0**: select an initial set of k points $\{z_i\}_{i=1}^k$, e.g., by using a Monte Carlo method; **Step 1**: select a $y \in \Omega$ at random, according to the probability density function $\rho(y)$; **Step 2**: find the z_i that is closest to y , and denote the index of that z_i by i^* ; **Step 3**: set $z_{i^*} \leftarrow \frac{j_{i^*} z_{i^*} + y}{j_{i^*} + 1}$ and $j_{i^*} \leftarrow j_{i^*} + 1$, then this new z_{i^*} along with the unchanged z_i , $i \neq i^*$, forms the new set of points $z_{i=1}^k$; **Step 4**: If this new set of points meets some convergence criteria, terminate; otherwise, go back to **Step 1**.

The K-means method has been analyzed in [35], where the almost sure convergence of energy is proved. Though attractive due to its simplicity, the convergence of the K-means method is very slow [11]. Nevertheless, the algorithm is highly amenable to fully scalable parallelization, as demonstrated in [22].

2.5 Sphere Packing

The CVT technique is an approximate method. In mathematics, there is an exact method based on sphere packing to tessellate the space. The standard packing problem is how to arrange spheres of equal radius to fill space as densely as possible in R^n . It is very hard to construct a packing scheme for an arbitrary n . Luckily, for the special cases, it has been proved that E_8 -lattice ($n = 8$) and Leech lattice ($n = 24$) give the densest lattice packing [7]. For E_8 -lattice, each lattice point has 240 nearest neighbors, and for Leech lattice the number is 196560 which is too large for our tessellation considering the sizes of common data. In more detail, for E_8 -lattice, the nearest neighbors of the origin have the shape $(\pm 1^2, 0^6)$ ($2^2 C_8^2 = 112$ of these) and $(\pm \frac{1}{2}^8)$ with even number of negative signs ($2^7 = 128$ of these). The set of neighbors Δ is actually the root lattice of E_8 -lattice since $E_8 = \mathbb{Z}\Delta$.

Though E_8 gives the densest packing in \mathbb{R}^8 , it may not be optimal restricted to a region with a fixed shape. Nevertheless, for a ball B in \mathbb{R}^8 , a possible tessellation scheme utilizing E_8 -lattice is that one point locates at the center of B , surrounded by 240 points in the way of E_8 within B . By adjusting the radius of packed spheres, we obtain a tessellation for B , which is symmetrical and has regions with exactly the same volume. Then if we tessellate the space with the tangent plane of each two spheres, we separate the space into regions with exactly the same volume rather than roughly equal one in a CVT.

3. TWAE

In this section, we follow the generalized formulation of generative auto-encoder with a reconstruction error in the data space and a discrepancy error in the latent space,

$$\min_{\phi, \psi} \mathbb{E}_{x \sim P_x} [c(x, \psi(\phi(x)))] + \lambda D(P_z || Q_z). \quad (15)$$

In Sec 3.1, to compute the discrepancy of P_z and Q_z more accurately, we first derive TWAE by tessellating the support of P_z and Q_z simultaneously. We further develop a new optimization strategy with non-identical batches as well as a regularizer to get better solutions in Sec 3.2.

3.1 Model Construction

In this paper, we propose P_z to be a uniform distribution in a unit ball, then the probability of a region is proportional to its volume. We adopt the Wasserstein distance as the divergence D for its good property though our tessellation framework is also flexible to other discrepancy metrics.

Let's go back to the discrete Wasserstein distance (1). Suppose there are N points of \tilde{z}_i sampled from the prior distribution P_z and the same number of z_i encoded by the encoder ϕ . P_N and Q_N are the empirical distribution of $\{\tilde{z}_i\}_{i=1}^N$ and $\{z_i\}_{i=1}^N$, respectively. We can compute the Wasserstein distance by assigning each z_i to a \tilde{z}_{σ_i} as follows

$$W(P_N, Q_N) = \frac{1}{N} \min_{\sigma} \sum_{i=1}^N \|z_i - \tilde{z}_{\sigma_i}\|, \quad (16)$$

where σ is a permutation of an index set $\{1, \dots, N\}$. It can be formulated as an assignment problem and solved by mature linear programming algorithms with a computational complexity of $O(N^{2.5} \log(N))$. Sinkhorn divergence can be a good alternative with a computational complexity of $\mathcal{O}(N^2/\epsilon^2)$, where ϵ stands for the accuracy of approximation [16]. However, when ϵ is small, this complexity is still prohibitive for the usage in the inner loop of a learning algorithm. As mentioned before, instead of linear programming, inaccurate approaches such as clipped networks [2] and random projection [9] have been proposed to address it. For large N , the traditional way is to divide the dataset into batches and to optimize the objective function batch by batch in a gradient descent manner, which is the well-known stochastic gradient descent. However, batches with small size lose some information to model the distribution delicately. To address this issue, we combine the assignment method and the batch optimization to a two-step algorithm. That is we first

design the batches according to their similarity and then minimize the discrepancy based on the optimization per batch.

For the first step, we find m points $\{\widehat{z}_j\}_{j=1}^m$ on the support of P_z . $\{\widehat{z}_j\}_{j=1}^m$ can be treated as generators of a tessellation $\{V_j\}_{j=1}^m$ on the support Ω that $V_i \cap V_j = \emptyset$ for $i \neq j$ and $\cup_{i=1}^k \overline{V}_i = \overline{\Omega}$. We assume that the volume of each V_j is equal so that we can sample a batch with the same number n of points in each V_j to model the distribution of P_z restricted on V_j . Assigning each encoded data point z_i to one of the generators $\{\widehat{z}_j\}_{j=1}^m$ is an easier task than (16) because m is much smaller than N . Each of $\{\widehat{z}_j\}_{j=1}^m$ is assigned by $n = \frac{N}{m}$ points. The problem can be formulated as

$$\begin{aligned}
 \min \quad & \sum_{i,j} \|z_i - \widehat{z}_j\|_2^2 f_{ij} \\
 \text{s.t.} \quad & \sum_{j=1}^m f_{ij} = 1, \quad i = 1, \dots, N \\
 & \sum_{i=1}^N f_{ij} = n, \quad j = 1, \dots, m \\
 & f_{ij} \in \{0, 1\}.
 \end{aligned} \tag{17}$$

It is a special case of the Hitchcock problem as both the demands and supplies are equal. By doing this, the dataset $\{z_i\}_{i=1}^N$ is clustered into m sets $\{S_j\}_{j=1}^m$ according to their distance to the generators $\{\widehat{z}_j\}_{j=1}^m$. Then for each cluster S_j corresponding to the generator \widehat{z}_j , we can estimate the Wasserstein distance of Q_z and P_z restricted on the region V_j .

The overall discrepancy is obtained by computing the local ones upon all the sets $\{S_j\}_{j=1}^m$. Thus, we have

$$\mathbb{E} [W_2^2(P_N, Q_N)] = \frac{1}{N} \mathbb{E} \left[\min_{\sigma} \sum_{i=1}^N \|z_i - \tilde{z}_{\sigma_i}\|_2^2 \right] \tag{18}$$

$$= \frac{1}{N} \mathbb{E} \left[\min_{\sigma} \sum_{j=1}^m \sum_{z_i \in S_j} \|z_i - \tilde{z}_{\sigma_i}\|_2^2 \right] \tag{19}$$

$$\leq \frac{1}{N} \mathbb{E} \left[\min_{\sigma} \sum_{j=1}^m \sum_{\substack{z_i \in S_j \\ \tilde{z}_{\sigma_i} \in V_j}} \|z_i - \tilde{z}_{\sigma_i}\|_2^2 \right] \tag{20}$$

$$\tag{21}$$

$$\begin{aligned}
 &= \frac{1}{N} \mathbb{E} \left[\sum_{j=1}^m \min_{\sigma^j} \sum_{\substack{z_i \in S_j \\ \tilde{z}_{\sigma_i^j} \in V_j}} \|z_i - \tilde{z}_{\sigma_i^j}\|_2^2 \right] \tag{22} \\
 &= \frac{1}{m} \mathbb{E} \left[\sum_{j=1}^m W_2^2(P_{n|V_j}, Q_{n|S_j}) \right], \tag{23}
 \end{aligned}$$

where $P_{n|V_j}$ denotes the empirical distribution of n samples of P_z restricted on V_j , $Q_{n|S_j}$ denotes the empirical distribution of S_j , σ^j denotes a permutation of an index set $\{1, \dots, n\}$ corresponding to the region V_j . The inequality in (20) is because the right side has more restriction that $\tilde{z}_{\sigma_i^j} \in V_j$. The equality in (22) is because z_i and $\tilde{z}_{\sigma_i^j}$ are restricted to S_j and V_j respectively. When $P_z = Q_z$, since S_j is a set of points which are the closest to \hat{z}_j and $\{V_j\}_{j=1}^m$ is CVT, then for a fixed $z_i \in S_j$, its optimal match \tilde{z}_{σ_i} in (19) belongs to V_j with high probability. If we fix m and let N approach infinity, the equality holds in (20). We assume that in the training procedure, $N \gg m$ and after a few iterations, Q_z and P_z are approximately equal so that we can optimize the subproblems on the right side of (23) instead.

We expect the sum of errors of estimates to the local discrepancies is smaller than the error on the whole support with the same estimator. We assume the total error can be divided into measurement error e_m and sampling error e_s . First, the measurement error denotes the error of the estimated Wasserstein distance. In general, the measurement error is a high-level minimum of the true discrete Wasserstein distance. As the sum of estimations on the regions is almost equal to that on the whole support, the sum of measurement errors (e_m) on regions should be smaller. Second, traditionally, we sample a batch of points from the whole distribution, so fewer points locate in a region of the support. Now we sample a batch in a local region to find the more subtle discrepancy and approximate the prior distribution better. Thus, the sampling error in local regions (e_s) is smaller. Our main results are that e_m and e_s decrease with rates of $\mathcal{O}(\frac{1}{\sqrt{m}})$ and $\mathcal{O}(\frac{1}{\sqrt{n}})$, respectively. We leave it to Section 4 for detailed theoretical exploration.

The whole scheme of the algorithm is summarized in **Algorithm 1**. Here we adopt the CVT technique to generate a proper tessellation. We compute CVT in the unit ball of the latent space to tessellate it into m regions with approximately equal volume. We follow the procedure of the Lloyd’s method and minimize the energy function in (14) to obtain the generators and a CVT. The CVT we computed is empirically good though it is not guaranteed to be the global minimum. The generators are fixed in the training process of the auto-encoder. The Hitchcock problem needs to be solved in each iteration, and it still costs too much to find the optimal solution. We adopt the least cost method (LCM) instead, which is a heuristic algorithm. We find the smallest admissible item d_{ij}^* of the distance matrix between $\{z_i\}_{i=1}^N$ and $\{\hat{z}_j\}_{j=1}^m$, and assign z_i to \hat{z}_i if \hat{z}_i is not saturated. The scheme of LCM is summarized in **Algorithm 2**. As to the discrepancy, we propose two non-adversarial methods based on the GW distance (4) and the SW distance (9). Both discrepancy metrics can be computed efficiently.

Algorithm 1 TWAE

Input: data $\{x_i\}_{i=1}^N$, CVT generators $\{\widehat{z}_i\}_{i=1}^m$, hyperparameter λ

Output: encoder ϕ , decoder ψ

```

1: repeat
2:    $z_i = \phi(x_i), i \in \{1, \dots, N\}$ 
3:   assign  $\{z_i\}$  to  $\{\widehat{z}_i\}$  by Algorithm 2 and obtain  $\{S_i\}_{i=1}^m$ 
4:   for  $k = 1 \rightarrow m$  do
5:     sample  $n$  points  $\{z_s^k\}$  in the region  $V_k$ 
6:     compute  $\mathcal{L}_{latent}^k = W(P_{n|V_k}, Q_{n|S_k})$ 
7:      $\mathcal{L}_{recons}^k = \sum_{x \in \{x_t | z_t \in S_k\}} \|x - \psi(\phi(x))\|$ 
8:     update  $\phi$  and  $\psi$  by minimizing  $\mathcal{L}^k = \mathcal{L}_{recons}^k + \lambda \mathcal{L}_{latent}^k$ 
9:   end for
10: until convergence
    
```

Algorithm 2 LCM

Input: encoded data $\{z_i\}_{i=1}^N$, generators $\{\widehat{z}_i\}_{i=1}^m$,

Output: clusters $S_i, i = 1, \dots, m$

```

1: compute the distant matrix  $M_{N \times m}$ 
2:  $S_i = \emptyset, i = 1, \dots, m$ 
3: repeat
4:   find the minimum item  $d_{ij}$  in  $M$ 
5:    $S_j = S_j \cup \{z_i\}$ 
6:   mask the  $i_{th}$  row in  $M$ 
7:   if  $|S_j| = n$  then
8:     mask the  $j_{th}$  column in  $M$ 
9:   end if
10: until all of  $\{z_i\}$  is assigned
    
```

3.2 Optimization with Non-identical Batches

In TWAE, the data points are separated into different batches according to their corresponding encoded representations in the latent space. Here $f(\theta)$ denotes the loss function of TWAE, θ denotes the parameters in the encoder and decoder, i.e.,

$$f(\theta) = \mathbb{E}_{x \sim P_x}[c(x, \psi(\phi(x)))] + \lambda D(P_z || Q_z). \quad (24)$$

Let $f_i(\theta)$ denote the loss function corresponding to the i -th batch of data. Thus, we have

$$f(\theta) = \sum_{i=1}^m f_i(\theta), \quad (25)$$

where m is the number of batches. In the setting of TWAE, since $f_i(\theta)$ and $f_j(\theta)$ ($i \neq j$) correspond to batches with different distributions, the value of $f_i(\theta)$ may increase with the

decrease of $f_j(\theta)$. This can result in instability for the autoencoder when it is optimized batch by batch. To solve this problem, we adopt a new optimization method attempting to keep the value of $f_i(\theta)$ ($i \neq j$) non-increasing when we optimize with the j -th batch of data.

Consider the first-order Taylor expansion of $f_i(\theta)$ with respect to $\bar{\theta}$

$$f_i(\theta) = f_i^{(1)}(\theta) + R_i(\theta), \quad (26)$$

where $f_i^{(1)}(\theta) = f_i(\bar{\theta}) + \nabla f_i(\bar{\theta})(\theta - \bar{\theta})$ and $R_i(\theta) = f_i(\theta) - f_i^{(1)}(\theta)$. Note that the optimization can be effective with the i.i.d. batches, which have similar loss function values. Inspired by this, to strengthen the similarity of $f_i(\theta)$ and $f_j(\theta)$ ($i \neq j$) in TWAE, we replace $R_i(\theta)$ and $R_j(\theta)$ to $R(\theta)$, where $R(\theta) = f(\theta) - f^{(1)}(\theta)$. Finally, the loss function of the i -th batch is $f_i^{(1)}(\theta) + \alpha R(\theta)$, where α is a hyper-parameter to balance the two terms. For the k -th iteration (corresponding to the k -th batch), the value of parameters is denoted by θ_k . The Taylor series of $f_k(\theta_k)$ is expanded with respect to θ_{k-1} . Thus the gradient of $f_k^{(1)}(\theta_k) + \alpha R(\theta_k)$ is

$$\begin{aligned} & \nabla_{\theta_k} \left(f_k^{(1)}(\theta_k) + \alpha R(\theta_k) \right) \\ &= \nabla_{\theta_k} \left(f_k(\theta_{k-1}) + \nabla_{\theta_{k-1}} f_k(\theta_{k-1})(\theta_k - \theta_{k-1}) \right) + \alpha \nabla_{\theta_k} \left(f(\theta_k) - f^{(1)}(\theta_k) \right) \\ &= \nabla_{\theta_{k-1}} f_k(\theta_{k-1}) + \alpha \nabla_{\theta_k} (f(\theta_k)) - \alpha \nabla_{\theta_k} \left(f^{(1)}(\theta_k) \right) \\ &= \nabla_{\theta_{k-1}} f_k(\theta_{k-1}) + \alpha \left[\nabla_{\theta_k} (f(\theta_k)) - \nabla_{\theta_{k-1}} (f(\theta_{k-1})) \right]. \end{aligned} \quad (27)$$

In practice, it is not convenient to compute $\nabla_{\theta_{k-1}} f_k(\theta_{k-1})$ with the k -th batch of data and parameters in the $(k-1)$ -th iteration, thus we compute $\nabla_{\theta_k} f_k(\theta_k)$ instead. For the second term $\alpha \left[\nabla_{\theta_k} (f(\theta_k)) - \nabla_{\theta_{k-1}} (f(\theta_{k-1})) \right]$, it is unrealistic to compute $\nabla f(\theta)$ as the number of data points is huge. Actually, the only thing that matters is the variation $\nabla_{\theta_k} (f(\theta_k)) - \nabla_{\theta_{k-1}} (f(\theta_{k-1}))$. We estimate $\nabla_{\theta_k} (f(\theta_k))$ and $\nabla_{\theta_{k-1}} (f(\theta_{k-1}))$ with the same batch randomly sampled from the whole dataset for better accuracy. To illustrate this, we have the following theorem.

Theorem 4 *Let $f_{S^{(k)}}(\theta_k)$ and $f_{S^{(k-1)}}(\theta_{k-1})$ be estimates to $f(\theta_k)$ and $f(\theta_{k-1})$ with random batches $S^{(k)}$ and $S^{(k-1)}$, respectively. Assume that f , $f_{S^{(k)}}$ and $f_{S^{(k-1)}}$ are two-time differentiable functions. Then the estimate error to the variation $\nabla_{\theta_k} (f(\theta_k)) - \nabla_{\theta_{k-1}} (f(\theta_{k-1}))$, i.e.,*

$$e = \left\| \left[\nabla_{\theta_k} (f_{S^{(k)}}(\theta_k)) - \nabla_{\theta_{k-1}} (f_{S^{(k-1)}}(\theta_{k-1})) \right] - \left[\nabla_{\theta_k} (f(\theta_k)) - \nabla_{\theta_{k-1}} (f(\theta_{k-1})) \right] \right\|_2, \quad (28)$$

is minimized when $S^{(k)} = S^{(k-1)}$.

Proof Let

$$F(S, \theta) \triangleq \nabla_{\theta} (f_S(\theta)) - \nabla_{\theta} (f(\theta)), \quad (29)$$

Algorithm 3 TWAE with regularization

Input: data $\{x_i\}_{i=1}^N$, CVT generators $\{\widehat{z}_i\}_{i=1}^m$, hyperparameter λ, α , learning rate γ
Output: encoder ϕ , decoder ψ

```

1: repeat
2:    $z_i = \phi(x_i), i \in \{1, \dots, N\}$ 
3:   assign  $\{z_i\}$  to  $\{\widehat{z}_i\}$  by Algorithm 2 and obtain  $\{S_i\}_{i=1}^m$ 
4:   for  $k = 1 \rightarrow m$  do
5:     compute  $\nabla_{\theta_k} (f_k(\theta_k))$  with  $S_k$ 
6:     sample  $S^{(k)}$  of  $n$  random points in  $\{z_i\}_{i=1}^N$ 
7:     compute  $\nabla_{\theta_k} (f_{S^{(k)}}(\theta_k))$  with  $S^{(k)}$ 
8:     if  $k=1$  then
9:        $g = \nabla_{\theta_k} (f_k(\theta_k))$ 
10:    else
11:      compute  $\nabla_{\theta_k} (f_{S^{(k-1)}}(\theta_k))$  with  $S^{(k-1)}$ 
12:       $g = \nabla_{\theta_k} (f_k(\theta_k)) + \alpha [\nabla_{\theta_k} (f_{S^{(k-1)}}(\theta_k)) - \nabla_{\theta_{k-1}} (f_{S^{(k-1)}}(\theta_{k-1}))]$ 
13:    end if
14:     $\theta_{k+1} = \theta_k - \gamma g$ 
15:  end for
16: until convergence

```

then we have

$$\begin{aligned}
 e &= \left\| [\nabla_{\theta_k} (f_{S^{(k)}}(\theta_k)) - \nabla_{\theta_{k-1}} (f_{S^{(k-1)}}(\theta_{k-1}))] - [\nabla_{\theta_k} (f(\theta_k)) - \nabla_{\theta_{k-1}} (f(\theta_{k-1}))] \right\|_2 \\
 &= \left\| [\nabla_{\theta_k} (f_{S^{(k)}}(\theta_k)) - \nabla_{\theta_k} (f(\theta_k))] - [\nabla_{\theta_{k-1}} (f_{S^{(k-1)}}(\theta_{k-1})) - \nabla_{\theta_{k-1}} (f(\theta_{k-1}))] \right\|_2 \\
 &= \left\| F(S^{(k)}, \theta_k) - F(S^{(k-1)}, \theta_{k-1}) \right\|_2 \\
 &= \mathcal{O}(\|S^{(k)} - S^{(k-1)}\|_2) + \mathcal{O}(\|\theta_k - \theta_{k-1}\|_2).
 \end{aligned} \tag{30}$$

The last equality is obtained by taking the first-order Taylor expansion of $F(S^{(k)}, \theta_k)$ with respect to $S^{(k-1)}$ and θ_{k-1} . Then e is minimized when $S^{(k)} = S^{(k-1)}$. \blacksquare

To conclude, the gradient in each iteration is computed with respect to two batches of data, i.e., one batch is restricted in a region for $\nabla_{\theta_k} f_k(\theta_k)$ and another batch is sampled from the whole support for $\nabla_{\theta_k} (f(\theta_k)) - \nabla_{\theta_{k-1}} (f(\theta_{k-1}))$. This optimization strategy is inspired by CEASE [14] and CSL [21] algorithms in distributed computing, where $f_i^{(1)}(\theta)$ is changed into $f^{(1)}(\theta)$ in each node machine under the assumption that data in different node machines are identically distributed. On the contrary, we assume the supports of distributions in different batches are disjoint, so we keep the first-order Taylor expansion unchanged to retain the differences. The algorithm of TWAE with regularization is summarized in **Algorithm 3**.

4. Theoretical Analysis

From a statistical view, the estimation of discrepancy by the discriminator in GAN is biased and of high variance. Since the discriminator has cumulative preferences of features when classify real and fake data, the estimates of discrepancy are somehow biased. Moreover, as of two-player setting, noise impedes drastically more the training compared to single objective one [6]. Thus, the variance is high. On the contrary, non-adversarial methods treat each data equally and have low variance on estimating the discrepancy. However, since non-adversarial methods are not accurate enough and not over-parameterized to memorize data, they suffer from errors, which are analysable. Suppose P_N and Q_N are empirical distributions of the sampled data $\{\tilde{z}_i\}_{i=1}^N$ and encoded data $\{z_i\}_{i=1}^N$, while P_n and Q_n denote the empirical distributions of batches with n points sampled from $\{\tilde{z}_i\}_{i=1}^N$ and $\{z_i\}_{i=1}^N$, respectively. We use $\widehat{W}(\cdot, \cdot)$ to denote the estimator of the true Wasserstein distance $W(\cdot, \cdot)$, then the error of estimation can be divided into sampling error e_s and measurement error e_m based on

$$\begin{aligned} \left| \widehat{W}(P_n, Q_n) - W(P_N, Q_N) \right| &\leq \left| W(P_n, Q_n) - W(P_N, Q_N) \right| \\ &+ \left| \widehat{W}(P_n, Q_n) - W(P_n, Q_n) \right| \\ &= e_s + e_m. \end{aligned} \tag{31}$$

In the following, we elaborate the superiority of the tessellation to reduce e_s and e_m respectively. We also analyze the computational complexity of TWAE in sampling and tessellation procedure.

4.1 Sampling Error

The target of generative models is to learn a continuous distribution. However, the road to continuity is discrete sampling. Points sampled randomly from the prior distribution are compared with the real data to make the encoder of auto-encoders or generator of GANs smooth in the latent space or the data space, respectively. Thus, while optimizing each batch, the task is to minimize the discrepancy of empirical distributions. Theorem 2 shows that the sampling error of the GW distance decreases with a rate of $\frac{1}{\sqrt{n}}$, we can also derive similar results for the SW distance.

Theorem 5 *Let P, Q is continuous distributions on \mathbb{R}^d . Let P_n and Q_n be generated by i.i.d. samples $z_1, \dots, z_n \sim Q$ and $\tilde{z}_1, \dots, \tilde{z}_n \sim P$ respectively. P'_n is an independent copy of P_n . Let*

$$J_2(P) = \int_{w \in S^{d-1}} \int_{F_w^{-1}(0)}^{F_w^{-1}(1)} \frac{F_w(x)(1 - F_w(x))}{p_w(x)} dx dw, \tag{32}$$

where p_w is the density of distribution P_w and P_w is the probability distribution $X^T w$ where $X \sim P$. F_w is the cumulative function of P_w . If $\max\{J_2(P), J_2(Q)\} < \infty$, then with n approaching infinity

$$\sqrt{n} (SW_2^2(P_n, Q_n) - SW_2^2(P, Q)) \rightarrow N(0, \sigma^2),$$

$$nSW_2^2(P_n, P'_n) \rightarrow \gamma_4,$$

where σ^2 is the variance correlated with P and Q , and γ_4 is a random variable correlated with P .

Proof It is a simple generalization of Theorem 3 by integrating on S^{d-1} . ■

Numerical test simulates the asymptotic property of the SW distance (Fig. 2) and we observe that $|SW_2^2(P_n, Q_n) - SW_2^2(P, Q)|$ and $SW_2^2(P_n, P'_n)$ decrease roughly via $\mathcal{O}\left(\frac{1}{\sqrt{n}}\right)$ and $\mathcal{O}\left(\frac{1}{n}\right)$, respectively. Then we can obtain upper bounds correlated with n , which are tighter than Claim 1 in Deshpande et al. [9],

$$\mathbb{E} [|SW_2^2(P_n, Q_n) - SW_2^2(P, Q)|] \leq \frac{C_1}{\sqrt{n}}, \quad (33)$$

$$\mathbb{E} [SW_2^2(P_n, P'_n)] \leq \frac{C_2}{n}, \quad (34)$$

where C_1 and C_2 are two constants.

At the end of this section, we illustrate the benefit of tessellation intuitively. Fix the number m of optimization step and the batch size n in each step. For $N = mn$, assume that the tessellation procedure induces an extra error which is no larger than $\mathcal{O}\left(\frac{1}{\sqrt{N}}\right)$, i.e.,

$$\frac{1}{m} \sum_{j=1}^m W_2^2(P_{n|V_j}, Q_{n|S_j}) = W_2^2(P_N, Q_N) + \mathcal{O}\left(\frac{1}{\sqrt{N}}\right). \quad (35)$$

Then the sampling error induced by the tessellated Wasserstein distance is of the same order with that of $W_2^2(P_N, Q_N)$, i.e., $\mathcal{O}\left(\frac{1}{\sqrt{N}}\right)$. If we sample empirical distributions of n points from P_N and Q_N for m times (denoted by $P_n^{(i)}$ and $Q_n^{(i)}$ for i -th time), then the sampling error induced by $\frac{1}{m} \sum_{i=1}^m W_2^2(P_n^{(i)}, Q_n^{(i)})$ is $\mathcal{O}\left(\frac{1}{\sqrt{n}}\right)$. One thing needs to clarify is that increasing the batch size n can also reduce the sampling error. However, it has drawbacks: 1) larger batch size leads to more consumption on both time and memory; the model optimized with large batch size may converge to saddle points [29], which may offset the reduction of sampling error. In other words, if we optimize with batches of size n on Ω , then after a few epochs, $W_2^2(P_n, Q_n)$ is approximately equal to $W_2^2(P_n, P'_n)$, where P'_n is an independent copy of P_n . This means we cannot identify Q from P with n sampled points. However, if we take a look at a region V_i with probability $P(V_i) = \frac{1}{m}$, we can still find differences between $P_{n|V_i}$ and $Q_{n|V_i}$ because in the past batches only a few points located in V_i and the sampling error was high. So the local information is lost in this way. On the contrary, TWAE samples a batch from each region, so that with the same size of batches, we can approximate the continuous distribution better. Numerical experiments in Section 5 demonstrate the effectiveness of this idea.

4.2 Measurement Error

In this section, we illustrate the optimality of using CVT in reducing the measurement error e_m in (31) and prove the descent rate of e_m with respect to the number of regions m in CVT is $\mathcal{O}\left(\frac{1}{\sqrt{m}}\right)$.

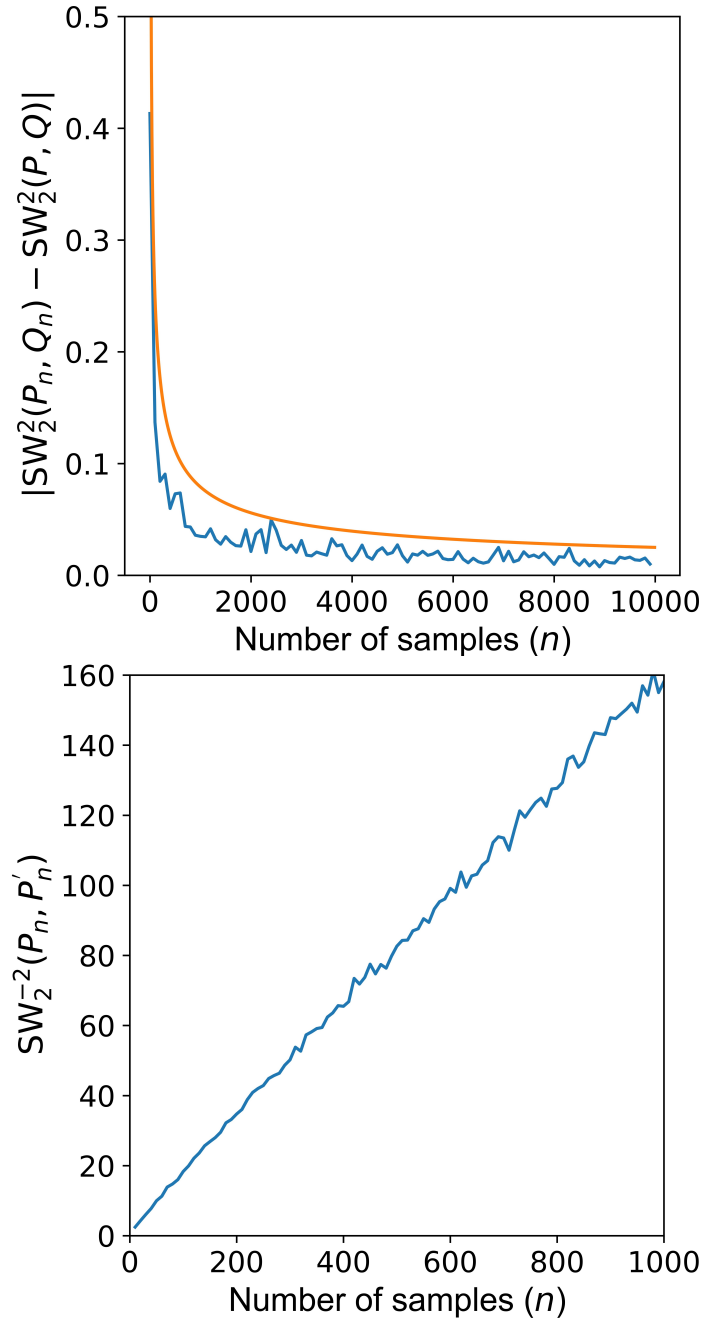


Figure 2: Illustration of the asymptotic property of the sliced-Wasserstein (SW) distance. Here P_n and P'_n are sampled from the same Gaussian distribution P of 64-dimension. Q_n is sampled from a uniform distribution in the unit ball of 64-dimension. $|SW_2^2(P_n, Q_n) - SW_2^2(P, Q)|$ is bounded by the orange line of $\frac{C}{\sqrt{n}}$, while the reciprocal of the SW distance $SW_2^{-2}(P_n, P'_n)$ increases linearly with n .

Let P_n and Q_n denote the empirical distribution of n points sampled from the prior distribution and the encoded data set, respectively. Both the SW and GW discrepancy metrics may lead to inaccurate estimation of the discrepancy. For the SW distance, we replace the integration in (9) over S^{d-1} with a summation over a randomly chosen set of unit vectors \widehat{S}^{d-1} . For the GW distance, we approximate P_n and Q_n with Gaussian distributions. To reduce the measurement error, we expect that the sum of errors for measuring the discrepancies on the tessellated supports is smaller than that on the whole support. For instance, if we approximate $P_n|_{V_j}$ with a Gaussian distribution in each region of Ω , we are actually utilizing a Gaussian mixture model to approximate P_N . A standard result in Bayesian nonparametrics says that every probability density is closely approximable by an infinite mixture of Gaussians. However, since the distribution in \mathbb{R}^d is no longer embeddable in the function space $L_p(0, 1)$ via quantile functions, it is hard to show the reduction of error with the increase of m . The extreme cases make the measurement error hard to analyze theoretically. To exclude the extreme cases, we unify the measurement error induced by different approaches with a parameter ϵ which depicts the estimator \widehat{W} .

Definition 1 Suppose P_n and Q_n are empirical distributions of n points. An estimator \widehat{W} is ϵ -good for (P_n, Q_n) if it holds that

$$|\widehat{W}_2^2(P_n, Q_n) - W_2^2(P_n, Q_n)| \leq \epsilon(\text{tr}(\Sigma(P_n)) + \text{tr}(\Sigma(Q_n))), \quad (36)$$

where $\Sigma(P_n)$, $\Sigma(Q_n)$ are the unbiased empirical covariance matrices of P_n and Q_n respectively, and $\text{tr}(\cdot)$ is the trace operator.

To explain the connection of $|\widehat{W}_2^2(P, Q) - W_2^2(P, Q)|$ and $\Sigma(P)$ and $\Sigma(Q)$, for instance, while adopting the GW distance as the estimator \widehat{W} , we use multivariate Gaussians to approximate P and Q , and ignore the information in the moments higher than two. Intuitively, by doing Taylor expansion on $|\widehat{W}_2^2(P, Q) - W_2^2(P, Q)|$, the loss of moments higher than two can be bounded by the variance of P and Q . More formally, we have the following theorem.

Theorem 6 $W_2^2(P_n, Q_n) \leq \frac{2(n-1)}{n-4} (\text{tr}(\Sigma(P_n)) + \text{tr}(\Sigma(Q_n)))$.

Proof First, using the triangle inequality, we have

$$\begin{aligned} W_2^2(P_n, Q_n) &= \min_{\sigma} \frac{1}{n} \sum_{i=1}^n \|z_i - \tilde{z}_{\sigma(i)}\|_2^2 \\ &= \min_{\sigma} \frac{1}{n} \sum_{i=1}^n \|z_i - \mathbb{E}_{z \sim P_n}[z] + \mathbb{E}_{z \sim P_n}[z] - \mathbb{E}_{z \sim Q_n}[z] + \mathbb{E}_{z \sim Q_n}[z] - \tilde{z}_{\sigma(i)}\|_2^2 \\ &\leq \frac{2}{n} \sum_{i=1}^n \|z_i - \mathbb{E}_{z \sim P_n}[z]\|_2^2 + \frac{2}{n} \sum_{i=1}^n \|\tilde{z}_i - \mathbb{E}_{z \sim Q_n}[z]\|_2^2 + 2\|\mathbb{E}_{z \sim P_n}[z] - \mathbb{E}_{z \sim Q_n}[z]\|_2^2 \\ &= \frac{2(n-1)}{n} (\text{tr}(\Sigma(P_n)) + \text{tr}(\Sigma(Q_n))) + 2\|\mathbb{E}_{z \sim P_n}[z] - \mathbb{E}_{z \sim Q_n}[z]\|_2^2. \end{aligned} \quad (37)$$

Note that

$$\begin{aligned}
 \|\mathbb{E}_{z \sim P_n}[z] - \mathbb{E}_{z \sim Q_n}[z]\|_2^2 &= \left\| \frac{\sum_{i=1}^n z_i}{n} - \frac{\sum_{i=1}^n \tilde{z}_i}{n} \right\|_2^2 \\
 &= \frac{1}{n^2} \left\| \sum_{i=1}^n (z_i - \tilde{z}_{\sigma(i)}) \right\|_2^2 \\
 &\leq \frac{2}{n^2} \min_{\sigma} \sum_{i=1}^n \|z_i - \tilde{z}_{\sigma(i)}\|_2^2 \\
 &= \frac{2}{n} W_2^2(P_n, Q_n).
 \end{aligned} \tag{38}$$

By taking (38) into (37), we have

$$W_2^2(P_n, Q_n) \leq \frac{2(n-1)}{n-4} (\text{tr}(\Sigma(P_n)) + \text{tr}(\Sigma(Q_n))). \tag{39}$$

■

In general, if the estimator is good, then the measurement error $|\widehat{W}_2^2(P, Q) - W_2^2(P, Q)|$ should be a high-level minim to the upper bound of $W_2^2(P, Q)$. Thus it is natural to assume \widehat{W}_2 satisfying (36) with a relatively small ϵ . With the assumption that \widehat{W}_2 is ϵ -good, we derive the optimality of using CVT in the setting of TWAE.

Theorem 7 *Let P be a uniform distribution on a compact and connected set Ω and Q is the target distribution. Assume that the optimal transport map \mathcal{T} from P to Q is continuously differentiable. Let $\{V_i\}_{i=1}^m$ be a tessellation on Ω . Assume that the estimator \widehat{W}_2 is ϵ -good for $\{(P_n|_{V_i}, \mathcal{T}_{\#}P_n|_{V_i})\}_{i=1}^m$.*

1. *The expectation of measurement error of the tessellated Wasserstein distance is upper bounded, i.e.,*

$$\mathbb{E}[e_m] \leq C_3 \sum_{i=1}^m \int_{V_i} \|z - \hat{z}_i\|_2^2 dz, \tag{40}$$

where \hat{z}_i is the mass centroid of V_i and C_3 is a constant correlated with Ω , ϵ and Q .

2. *A necessary condition for the right side of (40) to be minimized is that $\{V_i\}_{i=1}^m$ is the CVT and $\{\hat{z}_i\}_{i=1}^m$ is the generator set.*

Proof The measurement error of the tessellated Wasserstein distance can be formulated as

$$e_m = \sum_{i=1}^m P(V_i) \left| W_2^2(P_n|_{V_i}, \mathcal{T}_{\#}P_n|_{V_i}) - \widehat{W}_2^2(P_n|_{V_i}, \mathcal{T}_{\#}P_n|_{V_i}) \right|. \tag{41}$$

Since the estimator \widehat{W}_2 is ϵ -good, we have

$$\begin{aligned} e_m &\leq \epsilon \sum_{i=1}^m P(V_i) (\text{tr}(\Sigma(\mathcal{T}_{\#} P_{n|V_i})) + \text{tr}(\Sigma(P_{n|V_i}))) \\ &= \frac{\epsilon n}{n-1} \sum_{i=1}^m P(V_i) \mathbb{E}_{z \sim P_{n|V_i}} [\|\mathcal{T}(z) - \bar{\mathcal{T}}_i\|_2^2 + \|z - \bar{z}_i\|_2^2], \end{aligned} \quad (42)$$

where $\bar{z}_i = \mathbb{E}_{z \sim P_{n|V_i}}[z]$, $\bar{\mathcal{T}}_i = \mathbb{E}_{z \sim P_{n|V_i}}[\mathcal{T}(z)]$. Note that \mathcal{T} is continuously differentiable on the compact set Ω , then \mathcal{T} is Lipschitz continuous with a constant L . Thus

$$\mathbb{E}_{z \sim P_{n|V_i}} [\|\mathcal{T}(z) - \bar{\mathcal{T}}_i\|_2^2] \leq L^2 \mathbb{E}_{z \sim P_{n|V_i}} [\|z - \bar{z}_i\|_2^2]. \quad (43)$$

By taking (43) into (42), we obtain

$$\begin{aligned} e_m &\leq \frac{\epsilon n}{n-1} \sum_{i=1}^m P(V_i) (1 + L^2) \mathbb{E}_{z \sim P_{n|V_i}} [\|z - \bar{z}_i\|_2^2] \\ &= \frac{\epsilon n (1 + L^2)}{(n-1)|\Omega|} \sum_{i=1}^m |V_i| \mathbb{E}_{z \sim P_{n|V_i}} [\|z - \bar{z}_i\|_2^2]. \end{aligned} \quad (44)$$

The last equality is because P is a uniform distribution on Ω , thus $P(V_i) = \frac{|V_i|}{|\Omega|}$. Let $\tilde{z}_1^{(i)}, \dots, \tilde{z}_n^{(i)}$ be the support points of $P_{n|V_i}$, since they are randomly sampled from the uniform distribution on V_i , then

$$\begin{aligned} \mathbb{E}_{P_{n|V_i}} [\mathbb{E}_{z \sim P_{n|V_i}} [\|z - \bar{z}_i\|_2^2]] &= \mathbb{E}_{P_{n|V_i}} \left[\frac{1}{n} \sum_{k=1}^n \|\tilde{z}_k^{(i)} - \bar{z}^{(i)}\|_2^2 \right] \\ &= \frac{n-1}{n|V_i|} \int_{V_i} \|z - \hat{z}_i\|_2^2 dz, \end{aligned} \quad (45)$$

where $\hat{z}_i = \frac{1}{|V_i|} \int_{V_i} z dz$. Thus combining (45) and (44), we have

$$\begin{aligned} \mathbb{E}[e_m] &\leq \frac{\epsilon n (1 + L^2)}{(n-1)|\Omega|} \sum_{i=1}^m |V_i| \mathbb{E}_{P_{n|V_i}} [\mathbb{E}_{z \sim P_{n|V_i}} [\|z - \bar{z}_i\|_2^2]] \\ &= \frac{\epsilon (1 + L^2)}{|\Omega|} \sum_{i=1}^m \int_{V_i} \|z - \hat{z}_i\|_2^2 dz. \end{aligned} \quad (46)$$

Let $C_3 = \frac{\epsilon(1+L^2)}{|\Omega|}$, then we obtain the inequality in (40).

Next, we prove CVT is the necessary condition to minimize the upper bound in (40). First, fix the tessellation $\{V_j\}_{j=1}^m$, $\forall j \in \{1, \dots, m\}$

$$\int_{V_j} \|z - z_j^*\|_2^2 dz = \int_{V_j} (\|z\|_2^2 - 2z^T z_j^* + \|z_j^*\|_2^2) dz. \quad (47)$$

The integration is minimized when $z_j^* = \hat{z}_j = \frac{1}{|V_j|} \int_{V_j} z dz$. Second, fix \hat{z} and see what happens if $\{V_i\}_{i=1}^m$ is not a Voronoi tessellation generated by \hat{z} . Suppose that $\{\hat{V}_i\}_{i=1}^m$ is the Voronoi tessellation generated by \hat{z} . Since $\{V_i\}_{i=1}^m$ is not a Voronoi tessellation, there exists a particular value of $z \in V_i$, $\exists j \in \{1, \dots, m\}$ that

$$\|z - \hat{z}_j\|_2^2 < \|z - \hat{z}_i\|_2^2. \quad (48)$$

Thus,

$$\sum_{i=1}^m \int_{V_i} \|z - \hat{z}_i\|_2^2 dz > \sum_{i=1}^m \int_{\hat{V}_i} \|z - \hat{z}_i\|_2^2 dz. \quad (49)$$

So that the upper bound is minimized when $\{V_i\}_{i=1}^m$ is chosen to be the CVT and \hat{z} is the set of generators. \blacksquare

Theorem 8 *In the setting of Theorem 7, let $\{V_i^*\}_{i=1}^m$ and $\{\hat{z}_i^*\}_{i=1}^m$ be a tessellation on Ω and its generator set which minimize the right side of inequality (40), i.e.,*

$$\{V_i^*\}_{i=1}^m, \{\hat{z}_i^*\}_{i=1}^m \in \arg \min_{\{V_i\}_{i=1}^m, \{\hat{z}_i\}_{i=1}^m} C_3 \sum_{i=1}^m \int_{V_i} \|z - \hat{z}_i\|_2^2 dz, \quad (50)$$

then the expectation of e_m with respect to $\{V_i^*\}_{i=1}^m$ holds that

$$\mathbb{E}[e_m] \leq \frac{C_4}{\sqrt{m}}, \quad (51)$$

where C_4 is a constant correlated with Ω , ϵ and Q .

Proof Following the result in Theorem 7, we have

$$C_3 \sum_{i=1}^m \int_{V_i^*} \|z - \hat{z}_i^*\|_2^2 dz = C_3 \sum_{i=1}^m |V_i^*| \mathbb{E}_{P_n|V_i^*} \left[\mathbb{E}_{z \sim P_n|V_i^*} [\|z - \hat{z}_i^*\|_2^2] \right]. \quad (52)$$

Since (50) holds, following the result in Theorem 7, $\{V_i^*\}_{i=1}^m$ is a CVT and $\{\hat{z}_i^*\}_{i=1}^m$ is its generator. Let

$$\begin{aligned} P^* &= \sum_{i=1}^m \frac{|V_i^*|}{|\Omega|} P_n|_{V_i^*}, \\ Q^* &= \sum_{i=1}^m \frac{|V_i^*|}{|\Omega|} \delta_{\hat{z}_i^*}. \end{aligned} \quad (53)$$

Suppose \mathcal{T}_1 is the optimal transport map from P^* to Q^* , then let z belong to the support of $P_n|_{V_i^*}$, $\mathcal{T}_1(z) = \hat{z}_i^*$, which is held for $i = 1, \dots, m$. Thus, we have

$$\sum_{i=1}^m \frac{|V_i^*|}{|\Omega|} \mathbb{E}_{P_n|V_i^*} \left[\mathbb{E}_{z \sim P_n|V_i^*} [\|z - \hat{z}_i^*\|_2^2] \right] = \mathbb{E}_{P^*} [W_2^2(P^*, Q^*)]. \quad (54)$$

Since P^* is an empirical distribution, let P_m^* be an empirical distribution of m points i.i.d. sampled from P^* . Since (50) holds, we have

$$\begin{aligned} C_3 \sum_{i=1}^m \int_{V_i^*} \|z - \hat{z}_i^*\|_2^2 dz &= C_3 |\Omega| \mathbb{E}_{P^*} [W_2^2(P^*, Q^*)] \\ &\leq C_3 |\Omega| \mathbb{E}_{P^*} [\mathbb{E}_{P_m^*} [W_2^2(P^*, P_m^*)]]. \end{aligned} \quad (55)$$

For fixed P^* , according to Theorem 1, with m approaching infinity, $\sqrt{m}W_2^2(P^*, P_m^*)$ converges to a distribution. Since the support sets of P^* and P_m^* belong to Ω which is compact, then there exists a constant C'_4 such that

$$\mathbb{E}_{P^*} [\mathbb{E}_{P_m^*} [W_2^2(P^*, P_m^*)]] \leq \frac{C'_4}{\sqrt{m}}. \quad (56)$$

Let $C_4 = \frac{C'_4}{C_3|\Omega|}$, which is correlated with Ω , ϵ and Q . Finally, we obtain

$$\mathbb{E}[e_m] \leq C_3 \sum_{i=1}^m \int_{V_i^*} \|z - \hat{z}_i^*\|_2^2 dz \leq \frac{C_4}{\sqrt{m}}, \quad (57)$$

which completes the proof. ■

Since in the training procedure we need to define the tessellation $\{V_i\}_{i=1}^m$ before Q is known, the upper bound of error corresponding to $\{V_i\}_{i=1}^m$ is of importance. Theorem 7 gives the reason for utilizing the CVT technique and Theorem 8 shows that the error decreases with a rate of $\frac{1}{\sqrt{m}}$. Note that after a few iterations, Q is approximately equal to P , then the optimal transport map \mathcal{T} is almost identical. Thus, $\mathcal{T}(V_i) \approx V_i$ is a set of points that are closest to \hat{z}_i other than $\hat{z}_j (j \neq i)$. So the empirical distribution of S_i obtained by (17) is close to $\mathcal{T}_{\#}P_{n|V_i}$. Thus, in the algorithm, we compute $W(P_{n|V_i}, Q_{n|S_i})$ instead of $W(P_{n|V_i}, \mathcal{T}_{\#}P_{n|V_i})$. If $\{V_i\}_{i=1}^m$ is not a CVT, $\mathcal{T}_{\#}P_{n|V_i}$ and $Q_{n|S_i}$ will not coincide. The error induced by the approximation of $Q_{n|S_i}$ to $\mathcal{T}_{\#}P_{n|V_i}$ is hard to model. Nevertheless, it makes little effect on the results in the experiment.

4.3 Sampling and tessellation complexity

In TWAE, for an arbitrary z sampled from the uniform distribution on the unit ball in the latent space, we need to justify which region it belongs to by computing the distance between z and the generators of each region. The complexity of this is of order $\mathcal{O}(Nm)$. The tessellation complexity mainly arises in sorting the elements of the distance matrix M , which is $\mathcal{O}(Nm \log(Nm))$. Since we only sort the element of M once for N data points, the tessellation complexity $\mathcal{O}(Nm \log(Nm))$. By contrast, the sampling complexity of WAE is $\mathcal{O}(N)$. Though the complexity of TWAE is higher than that of WAE, the time consumption of LCM on CPU is comparable to that of the backpropagation algorithm on GPU (Table 1).

5. Experimental Results

In this section, we numerically evaluate TWAE from five aspects. In section 5.3, we compare TWAE with related studies. In section 5.4, we test the optimization method introduced in section 3. In section 5.5, we compare the performance of the CVT technique and sphere packing. In section 5.6, we compare the models with and without tessellation. We test TWAE with the GW distance (TWAE-GW) and the SW distance (TWAE-SW) respectively on two real-world datasets including MNIST [27] consisting of 70k images and CelebA [33] consisting of about 203k images. Finally, in section 5.7, we test TWAE with other SW distances such as DSW, Max-SW and GSW distances on LSUN-Bedrooms dataset [47]. We use the Fréchet inception distance (FID) introduced by Heusel et al. [19] to measure the quality of the generated images. Smaller FID indicates better quality.

5.1 Architectures for different datasets

For MNIST, we use a simple auto-encoder consisting of a mirrored deep convolutional neural network with ReLU as the activation function to compare the performance of the CVT technique and sphere packing (Section 5.5).

Encoder architecture:

$$\begin{aligned} x \in \mathcal{R}^{28 \times 28} &\rightarrow \text{Conv}_{128} \rightarrow \text{BN} \rightarrow \text{ReLU} \\ &\rightarrow \text{Conv}_{256} \rightarrow \text{BN} \rightarrow \text{ReLU} \\ &\rightarrow \text{Conv}_{512} \rightarrow \text{BN} \rightarrow \text{ReLU} \\ &\rightarrow \text{Conv}_{1024} \rightarrow \text{BN} \rightarrow \text{ReLU} \rightarrow \text{FC}_8. \end{aligned}$$

Decoder architecture:

$$\begin{aligned} z \in \mathcal{R}^8 &\rightarrow \text{FC}_{7 \times 7 \times 1024} \\ &\rightarrow \text{FSConv}_{512} \rightarrow \text{BN} \rightarrow \text{ReLU} \\ &\rightarrow \text{FSConv}_{256} \rightarrow \text{BN} \rightarrow \text{ReLU} \rightarrow \text{FSConv}_1. \end{aligned}$$

For CelebA, we use two architectures A and B with different sizes of parameters to test if TWAE shows consistent results under different architectures (Fig. 3). Numerical experiments show that our tessellation technique is effective on both architectures. The FID score decreases rapidly when the number of regions m is lower than 100. However, there is no more decline when m is larger. Architecture A is similar to that of Tolstikhin et al. [43] and is used to compare the performance of TWAE with other generative auto-encoders fairly (Section 5.3).

Encoder of architecture A:

$$\begin{aligned} x \in \mathcal{R}^{64 \times 64 \times 3} &\rightarrow \text{Conv}_{128} \rightarrow \text{BN} \rightarrow \text{ReLU} \\ &\rightarrow \text{Conv}_{256} \rightarrow \text{BN} \rightarrow \text{ReLU} \\ &\rightarrow \text{Conv}_{512} \rightarrow \text{BN} \rightarrow \text{ReLU} \\ &\rightarrow \text{Conv}_{1024} \rightarrow \text{BN} \rightarrow \text{ReLU} \rightarrow \text{FC}_{64}. \end{aligned}$$

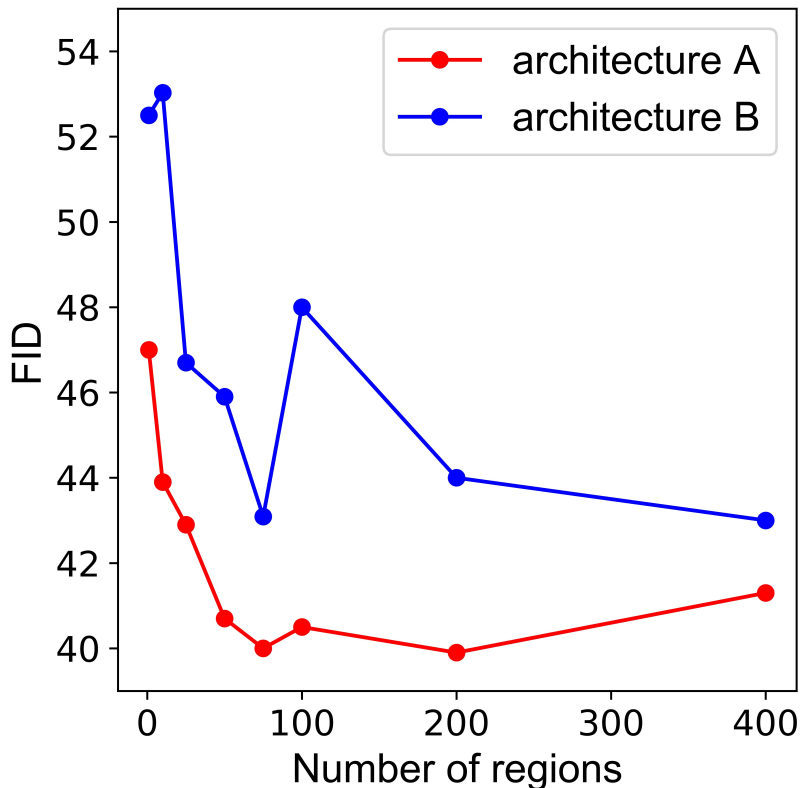


Figure 3: Comparison of changing trend of FID scores versus the number of regions m . Here m are set to 1 (without tessellation), 10, 25, 50, 75, 100, 200, 400 for both architectures A and B.

Decoder of architecture A:

$$\begin{aligned}
 z \in \mathcal{R}^{64} &\rightarrow \text{FC}_{8 \times 8 \times 1024} \\
 &\rightarrow \text{FSConv}_{512} \rightarrow \text{BN} \rightarrow \text{ReLU} \\
 &\rightarrow \text{FSConv}_{256} \rightarrow \text{BN} \rightarrow \text{ReLU} \\
 &\rightarrow \text{FSConv}_{128} \rightarrow \text{BN} \rightarrow \text{ReLU} \rightarrow \text{FSConv}_3.
 \end{aligned}$$

Architecture B has the same number of layers and half the number of nodes. For less computational cost, we use architecture B to investigate the properties of TWAE extensively (Sections 5.4 and 5.6). For LSUN-Bedrooms, we use architecture A since the size of this dataset is much larger than those of CelebA and the MNIST (Section 5.7).

Encoder of architecture B:

$$\begin{aligned}
 x \in \mathcal{R}^{64 \times 64 \times 3} &\rightarrow \text{Conv}_{64} \rightarrow \text{BN} \rightarrow \text{ReLU} \\
 &\rightarrow \text{Conv}_{128} \rightarrow \text{BN} \rightarrow \text{ReLU} \\
 &\rightarrow \text{Conv}_{256} \rightarrow \text{BN} \rightarrow \text{ReLU} \\
 &\rightarrow \text{Conv}_{512} \rightarrow \text{BN} \rightarrow \text{ReLU} \rightarrow \text{Conv}_{64}.
 \end{aligned}$$

	LCM			BP	
	$m = 100$	$m = 200$	$m = 400$	Architecture A	Architecture B
$N = 4000$	1.43 (0.02)	2.87 (0.01)	7.11 (0.07)	15.67 (0.08)	3.35 (0.01)
$N = 10000$	7.71 (0.02)	24.34 (0.04)	50.67 (0.16)	39.30 (0.11)	6.75 (0.02)
$N = 20000$	47.06 (0.01)	96.56 (1.25)	198.07 (1.27)	78.34 (1.42)	13.49 (0.03)

Table 1: Comparison of time cost between LCM on CPU and BP on GPU (seconds)

Decoder of architecture B:

$$\begin{aligned}
 z \in \mathcal{R}^{64} &\rightarrow \text{FSConv}_{512} \rightarrow \text{BN} \rightarrow \text{ReLU} \\
 &\rightarrow \text{FSConv}_{256} \rightarrow \text{BN} \rightarrow \text{ReLU} \\
 &\rightarrow \text{FSConv}_{128} \rightarrow \text{BN} \rightarrow \text{ReLU} \\
 &\rightarrow \text{FSConv}_{64} \rightarrow \text{BN} \rightarrow \text{ReLU} \rightarrow \text{FSConv}_3.
 \end{aligned}$$

5.2 Experimental setup

The hyperparameter λ of the auto-encoder in (11) is set to 1 for SW distance and 0.01 for GW, GSW and DSW distance. The dimensionalities of the latent space are set to 8 for MNIST, 64 for CelebA and 128 for LSUN-Bedrooms, respectively. The number 241 of root lattices of E_8 -lattice is chosen for sphere packing test. How many data points (N) in the training dataset should be used for one single tessellation is a question. In the traditional setting, the data is shuffled in each epoch to prevent overfitting. If we take N as large as the size of the training dataset, the designed batches in each epoch will be approximately the same, which leads to bad generalization. Thus, larger N may not perform better. We tried various values of N and noticed that $N = 10000$ or 20000 work well. Compared with traditional algorithms, the only extra computation is using LCM to solve the Hitchcock problem to design batches for each data. The time cost of LCM on CPU is comparable to that of backpropagation algorithm (BP) on GPU (Table 1). We implement our algorithms on Pytorch with the Adam optimizer.

5.3 TWAE can generate high-quality images

We first test if TWAE can approximate the support of the distribution of real data with a smooth and well-learned manifold by interpolations, test reconstruction, and random generating (Fig. 4). For interpolation, considering the probability concentrated near the surface of the unit ball, we interpolate on the curve near the surface instead of linear interpolation to avoid interpolating near the origin. In our experiments, the transition of the decoder from one point to another in the latent space is smooth and gradual. For reconstruction, TWAE can reconstruct the test data which means the model generalizes well. For random generating, samples are generated by sampling in the unit ball uniformly and transforming the resulting vector z into an image via the decoder. By generating images of good quality, the ‘‘hole’’ in the latent space is filled and TWAE indeed generate a well-learned manifold. We also compared the performance of TWAE with WAE-GAN,



Figure 4: Comparison of interpolated, reconstructed and generated images by TWAE.

WAE-MMD [43], SWAE and VAE. Only WAE-GAN has a discriminator. We use the results in Tolstikhin et al. [43]; Kolouri et al. [25] since the architectures of these networks are similar, and it is not easy to reproduce the results of WAE-GAN. TWAE shows very competitive performance compared to WAE-GAN (Table 2).

Model	FID
TWAE-SW	39.9
TWAE-GW	44.5
VAE	63
WAE-MMD	55
SWAE	79
WAE-GAN	42

Table 2: Performance comparison of different methods on CelebA

5.4 The non-identical batch optimization is effective

We set three different numbers of regions (i.e., $m = 100, 200, 400$) for both MNIST and CelebA. Numerical results show that the FID score decreases with larger m on MNIST, while it doesn't change significantly on CelebA (Table 3). The difference is probably due to the diverse complexity of the two datasets. We note that the distribution of each batch is different as we put similar data into a batch. The discrepancy of different batches is larger with relatively smaller batch sizes. To address this issue, we propose the non-identical batch optimization method (Section 3) by adding a regularizer for better generalization. Here the hyperparameter α is set to 0.2. Numerical results of TWAE with the regularizer indeed show better performance than without it with different ms for most cases (Table 3). The only exception is that for the GW distance with $m = 200$ and 400 respectively, which is explained in Section 5.7.

5.5 The CVT technique gets similar performance with the exact model

The CVT technique is an iterative and approximate algorithm that can be adjusted to any dimensions. The iteration is based on integrating over each region. The computation goes up exponentially as the dimension increases. So the CVT technique may not be accurate enough in high-dimensional cases. Thus, it is necessary to explore the effect of it. We implement TWAE with exact lattices and compare its performance with that of the CVT technique. For the MNIST dataset, the dimension of the latent space is 8. Numerical results show that the CVT technique achieves comparable performance and gets very similar FID score with the sphere packing E_8 -lattice dividing into 241 regions (Fig. 5), indicating that it gets similar performance with the exact model.

5.6 Tessellation indeed improve the performance of generation

Here we show that our tessellation procedure can indeed enhance the performance of non-adversarial methods using existing discrepancy metrics, such as the SW and GW distance.

MNIST				
	TWAE-SW	TWAE-SW(r)	TWAE-GW	TWAE-GW(r)
$m = 100$	20.4	16.3	18.0	15.9
$m = 200$	17.5	16.0	15.7	14.3
$m = 400$	15.6	13.9	14.2	13.8
CelebA				
	TWAE-SW	TWAE-SW(r)	TWAE-GW	TWAE-GW(r)
$m = 100$	49.2	47.8	46.7	44.5
$m = 200$	50.2	44.1	47.2	48.1
$m = 400$	47.2	43.5	54.0	57.2

Table 3: Performance comparison of TWAE with or without regularizer on MNIST and CelebA with three given numbers of regions

When measure the distance of the two distributions with the GW distance, we treat P_z and Q_z as multivariate Gaussian and ignore the information in the high-order moment. Thus, the approximation is not very good. But with the tessellation technique, actually, we are using a Gaussian mixture distribution with each component in a region to approximate the target distribution. With tessellation, it can be better than the state of the art non-adversarial auto-encoders. Furthermore, for the more accurate discrepancy metrics such as the SW distance, we achieve better performance (Table 4). In Fig. 6, we show the downward trends with and without tessellation in the training progress to prove that TWAE has superior generative performance, while keeping the good property of stability. However, for the SW distance, since the decoder of an auto-encoder is only trained with the reconstruction loss, it may not generalize to the “hole” between the training points. This means increasing the number of regions can not go beyond the generalization ability of the decoder. For instance, the improvements from 200 regions to 400 regions is fewer than that from 100 regions to 200 regions. For the GW distance, when the batch size is smaller than the dimension of the latent space, the computation of $(\Sigma_2^{1/2}\Sigma_1\Sigma_2^{1/2})^{1/2}$ in (4) is ill-posed. Consequently, the FID score doesn’t decrease notably as expected in the case of batch size = 50 and 25. Furthermore, TWAE is robust to the hyperparameter λ . In the case when λ is 100 times larger than default (Fig. 7), TWAE-GW can generate distinctly better images (FID=54.8) than without tessellation (FID=74.8).

In Fig. 8, we show that, at the end of the training procedure, the SW distance can not identify Q_n from P_n , i.e., $SW(Q_n, P_n)$ converges to $SW(P_n, P'_n)$, where P'_n is sampled from the same P_z as P_n . However, in the regions of the whole support, the discrepancy of P_z and Q_z still exists. With tessellation, the SW distance in the regions are closer to sampling from the same distribution, indicating that the tessellation could further reduces the discrepancy.

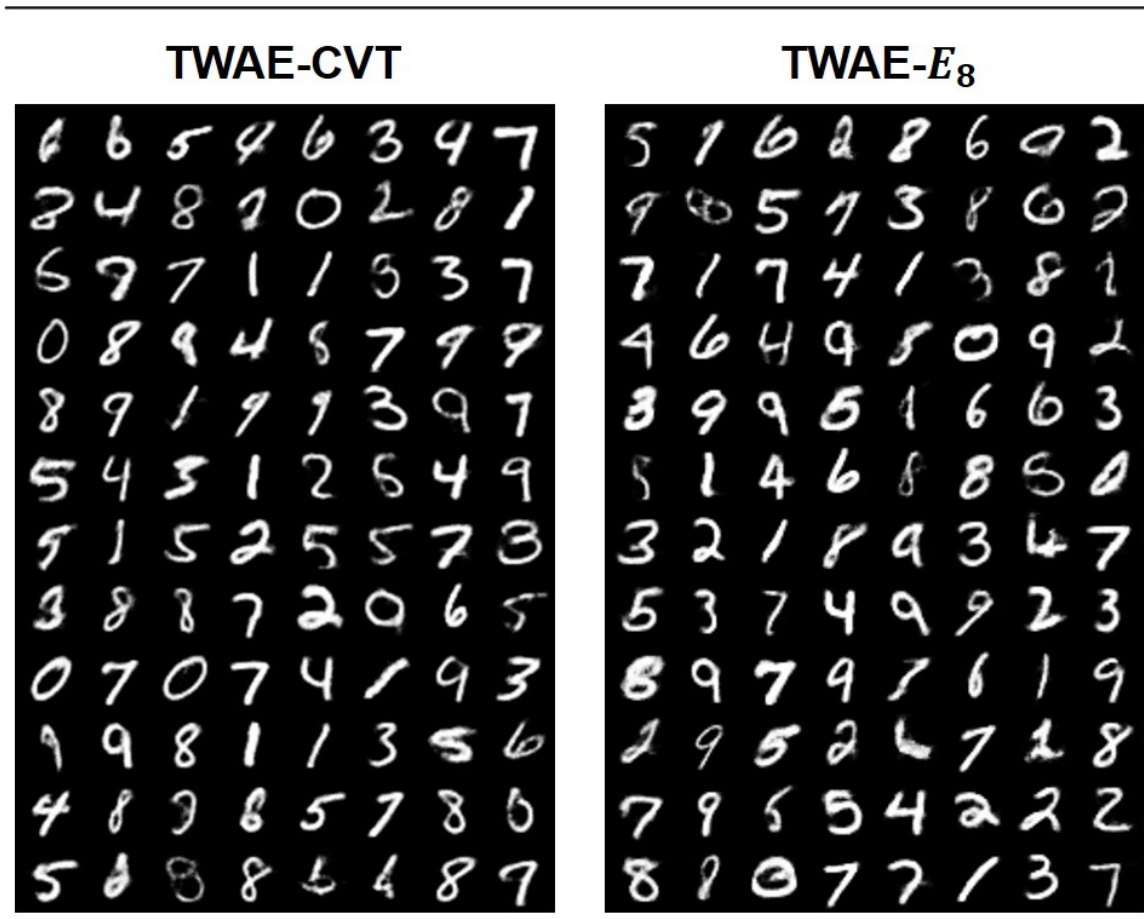


Figure 5: Comparison of generated images of TWAE with CVT and E_8 -lattice. The FID scores of them are 16.8 and 16.9 respectively.

distance (batch size)	with tessellation	without tessellation
SW (100)	48.5	52.5
SW (50)	43.8	51.1
SW (25)	43.4	51.5
GW (100)	44.5	51.2
GW (50)	48.1	50.1
GW (25)	57.2	58.6

Table 4: Comparison of TWAE with and without tessellation

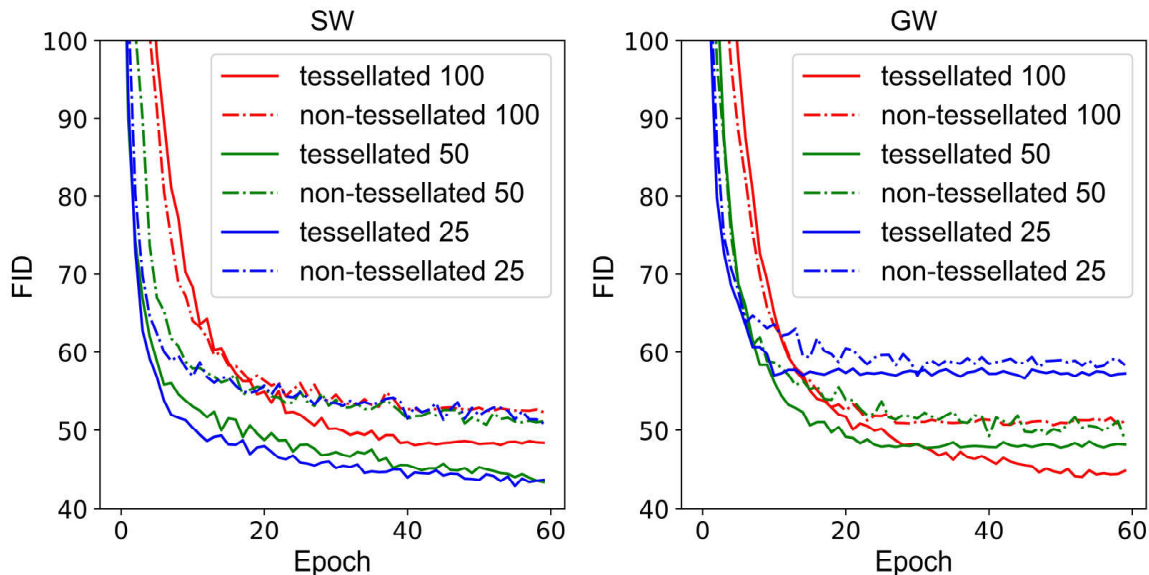


Figure 6: Comparison of changing trend of FID scores versus training epochs between models with and without tessellation for both SW and GW distances. N is set to be 10000 in this experiment. $m = 100, 200, 400$ are used for tessellation, and correspondingly the batch sizes are set to 100, 50, 25 for models without tessellation, respectively.

5.7 TWAE with other SW distances

In this subsection, we test TWAE with several recent proposals of SW distances (Max-SW, GSW and DSW) on LSUN-Bedrooms to show its power in enhancing performance of generative auto-encoders. For TWAE, we set $N = 10000$ and $m = 100$. For GSW, we use circular function to compute the distance. For Max-SW and DSW, the numbers of iterations to find the optimal projection and the optimal distribution of projection are both set to 10. The numbers of projections are all set to 1000 for SW, DSW and GSW respectively.

Model	FID	Model	FID
TWAE-SW	193.2	WAE-SW	205.4
TWAE-GSW	193.7	WAE-GSW	214.1
TWAE-DSW	196.3	WAE-DSW	210.3

Table 5: Performance comparison of the SW, GSW and DSW distances on the LSUN-Bedrooms dataset.

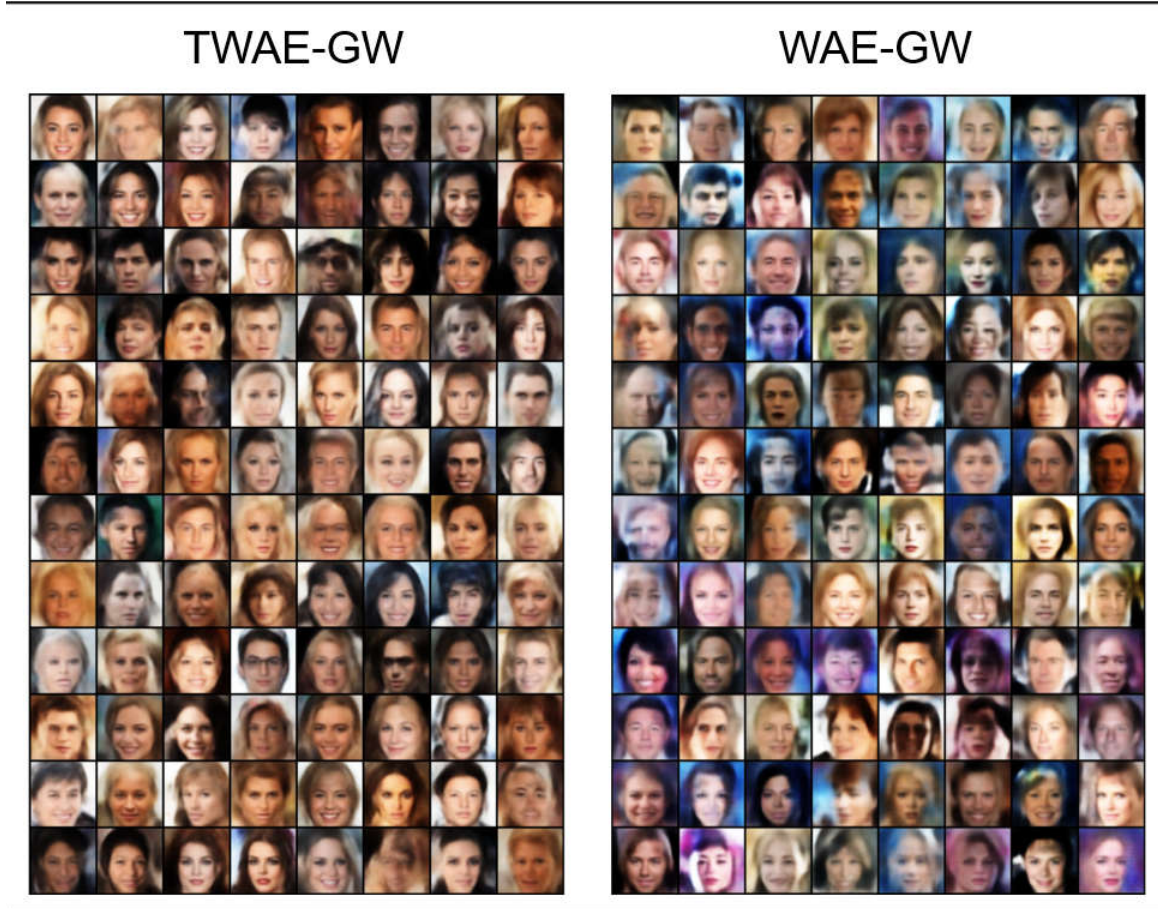


Figure 7: Comparison of generated images using TWAE-GW and WAE-GW with $\lambda=1$ (100 times larger than default). The FID scores of TWAE-GW and WAE-GW are 54.8 and 74.8 respectively.

As we expected, the tessellation technique can enhance the performance of auto-encoders with SW, GSW and DSW uniformly (Table 5). The performance of TWAE-SW, TWAE-GSW and TWAE-DSW are very similar, while the performance of WAE-GSW and WAE-DSW is even slightly worse than that of WAE-SW. This is because DSW is designed for GAN, in which the latent distributions are complex and anisotropic. A few of projection samples in SW are more important than the rest. DSW finds an optimal distribution of important projection samples, which leads to better performance in GAN. Also, GSW is designed to model the irregular support shape of the latent distribution. However, in the setting of auto-encoder, when the prior latent distribution is uniform in a unit ball, each projection samples contributes equally in SW and the support shape of latent distribution is regular. Thus, SW is better than GSW and DSW for WAE. It should be noted that Max-SW finds the most important projection sample, but ignores the rest which is still

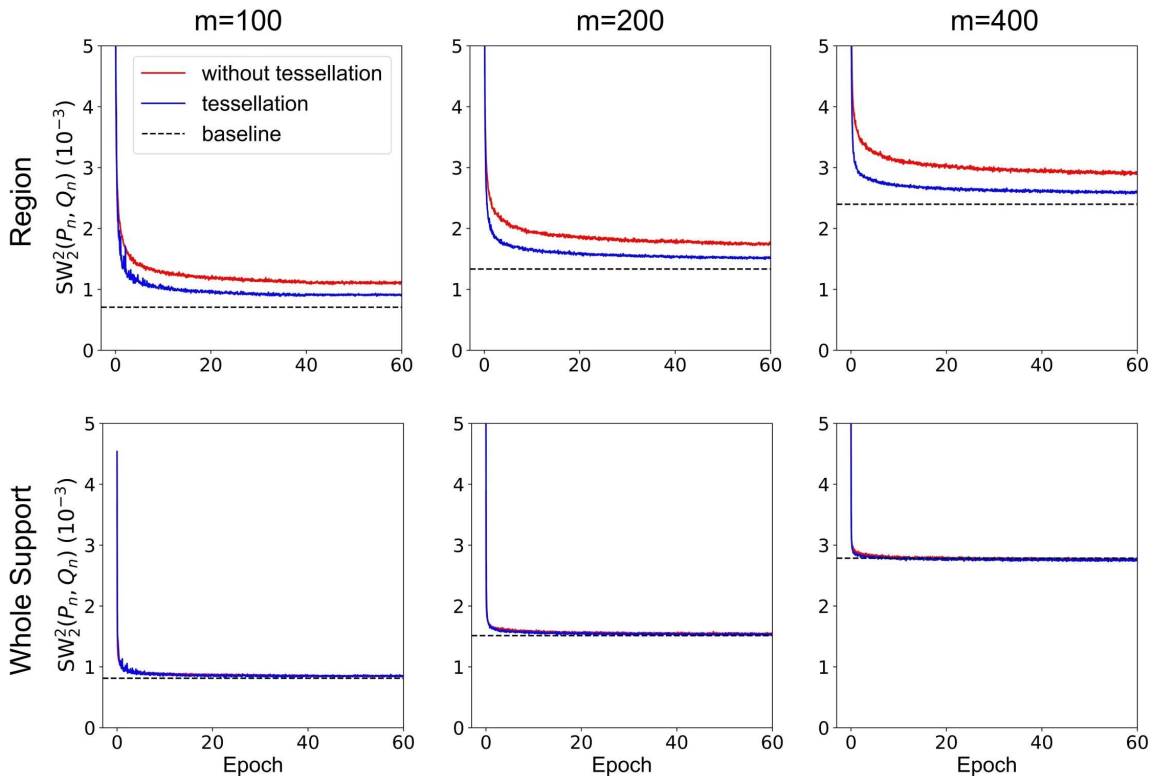


Figure 8: Comparison of the SW distance in the training procedure with tessellation $m = 100, 200, 400$ and without tessellation. The baseline is the SW distance of two sets of points sampled from a uniform distribution in the unit ball (the whole support) or in the regions.

important due to the isotropic latent distribution. Thus, WAE and TWAE with Max-SW fail to learn the distribution and don't converge in this test.

6. Discussion and Conclusion

In this paper, we propose a novel non-adversarial generative framework TWAE, which designs batches according to data similarity instead of random shuffling, and optimizes the discrepancy locally. It shows very competitive performance to an adversarial generative model WAE-GAN, while sharing the stability of other non-adversarial ones. It is very flexible and applicable to different discrepancy metrics to enhance their performance. To our knowledge, TWAE is the first generative model to design batches and optimize with non-identical distributions. To this end, we use a computational geometry technique CVT, which is often used in three-dimensional modeling, and develop a new optimization method to deal with such non-identical batches. TWAE can generate images of higher quality in terms of FID score with relatively more regions when the computing resource is adequate.

TWAE is designed to learn the data distribution in the latent space learned by an auto-encoder model, instead of the original space ($d > 1000$) of data (e.g., images). Generally, the distribution of data concentrates near a low-dimension manifold, so the similarity should be measured by the Riemann metric on the manifold rather than the Euclidean metric. However, construction of the Riemann metric in high dimensional space without neural network is hard. Thus, we suggest to tessellate the latent space to approximate the target distribution better. Here we suggest to use the uniform distribution but not the i.i.d. Gaussian as the prior distribution of the latent space. The reasons for this are threefold: 1) for a uniform distribution, the probability of a region $P(V_i)$ is corresponding to its volume. It is convenient to conduct tessellation with equal-weighted sampling; 2) uniform distribution is isotropic when restricted to a region. While computing the SW distance, projections of different directions have useful information because the distribution is isotropic; 3) when the points obey uniform distribution, we can use the Euclidean metric to measure the similarity of two points.

Since the decoder ψ is trained on Q_z rather than P_z , the quality of generated images may not be as good as that of GAN. In some situations, people care about generating more than encoding. It is nontrivial to generalize the tessellation technique to GAN. The reason for this is two-fold: 1) The adversarial mechanism is unstable and sensitive to noise, thus the variance induced by such designed batches may impede the optimization process of GAN; 2) In GAN, there is no encoder to extract high-level representation of data, which makes it difficult to cluster the data into batches according to their similarity. Nevertheless, it will be valuable to develop a technique analogous to tessellation that can enhance the performance of GAN.

In TWAE, since the supports of distributions of different batches are disjoint, the model does not forget the information in passed batches when learn with a new batch. However, neural network tends to forget the knowledge of previously learned tasks as information relevant to the current task is incorporated. This phenomenon is termed catastrophic forgetting. For instance, in the situations of online machine learning, data becomes available in sequential order. So the distribution of each batch may change, and previously learned knowledge might lose. Numerical experiments showed that our optimization method can deal with non-identical batches, i.e., learning from the current batch without forgetting the former batches. Can techniques in catastrophic forgetting help to further reduce the gap of the SW distance in the regions (Fig. 8)? Or can our non-identical batch optimization help to overcome the catastrophic forgetting? They will be valuable questions worthing further studying.

As mentioned above, the numbers of minimal vectors of E_8 -lattice and Leech lattice for 8- and 24-dimension cases are 240 and 196560 respectively. So the data we have actually can not fill the latent space when the dimension is very high. Some bad images will be generated when we randomly sample in the latent space due to the lack of data points. Unfortunately, there is no criterion to judge whether the sampled point in the latent space can generate a good image. In the future, how to build the statistics to evaluate the quality of the generated images and find the well-learned region in the latent space is an important topic.

Acknowledgments

This work has been partially supported by the National Key R&D Program of China [2019YFA0709501]; the National Natural Science Foundation of China [61621003]; National Ten Thousand Talent Program for Young Top-notch Talents; CAS Frontier Science Research Key Project for Top Young Scientist [QYZDB-SSW-SYS008].

References

- [1] Martin Arjovsky and Léon Bottou. Towards principled methods for training generative adversarial networks. *International Conference on Learning Representations*, pages 1–14, 2017.
- [2] Martin Arjovsky, Soumith Chintala, and Léon Bottou. Wasserstein generative adversarial networks. In *Proceedings of the 34th International Conference on Machine Learning*, volume 70, pages 214–223, 2017.
- [3] Sanjeev Arora, Rong Ge, Yingyu Liang, Tengyu Ma, and Yi Zhang. Generalization and equilibrium in generative adversarial nets (gans). In *Proceedings of the 34th International Conference on Machine Learning*, volume 70, pages 224–232, 2017.
- [4] Sergey Bobkov and Michel Ledoux. One-dimensional empirical measures, order statistics and kantorovich transport distances. *Memoirs of the American Mathematical Society*, pages 1–140, 2016.
- [5] Nicolas Bonnotte. *Unidimensional and evolution methods for optimal transportation*. PhD thesis, Paris 11, 2013.
- [6] Tatjana Chavdarova, Gauthier Gidel, François Fleuret, and Simon Lacoste-Julien. Reducing noise in gan training with variance reduced extragradient. *Advances in Neural Information Processing Systems*, pages 391–401, 2019.
- [7] Henry Cohn, Abhinav Kumar, Stephen D Miller, Danylo Radchenko, and Maryna Viazovska. The sphere packing problem in dimension 24. *Annals of Mathematics*, pages 1017–1033, 2017.
- [8] Marco Cuturi. Sinkhorn distances: Lightspeed computation of optimal transport. *Advances in Neural Information Processing Systems*, 26:2292–2300, 2013.
- [9] Ishan Deshpande, Ziyu Zhang, and Alexander Schwing. Generative modeling using the sliced wasserstein distance. In *Proceedings of the IEEE Conference on Computer Vision and Pattern Recognition*, pages 3483–3491, 2018.
- [10] Ishan Deshpande, Yuan-Ting Hu, Ruoyu Sun, Ayis Pyrros, Nasir Siddiqui, Sanmi Koyejo, Zhizhen Zhao, David Forsyth, and Alexander G Schwing. Max-sliced wasserstein distance and its use for gans. In *Proceedings of the IEEE Conference on Computer Vision and Pattern Recognition*, pages 10648–10656, 2019.

- [11] Qiang Du and Tak-Win Wong. Numerical studies of macqueen’s k-means algorithm for computing the centroidal voronoi tessellations. *Computers & Mathematics with Applications*, 44(3-4):511–523, 2002.
- [12] Qiang Du, Vance Faber, and Max Gunzburger. Centroidal voronoi tessellations: Applications and algorithms. *SIAM Review*, 41(4):637–676, 1999.
- [13] Pavel Dvurechensky, Alexander Gasnikov, and Alexey Kroshnin. Computational optimal transport: Complexity by accelerated gradient descent is better than by sinkhorn’s algorithm. *International Conference on Machine Learning*, pages 1–10, 2018.
- [14] Jianqing Fan, Yongyi Guo, and Kaizheng Wang. Communication-efficient accurate statistical estimation. *CoRR abs/1906.04870*, 2019.
- [15] Yuan Gao, Jian Huang, Yuling Jiao, and Jin Liu. Learning implicit generative models with theoretical guarantees. *CoRR abs/2002.02862*, 2020.
- [16] Aude Genevay, Gabriel Peyré, and Marco Cuturi. Learning generative models with sinkhorn divergences. *International Conference on Artificial Intelligence and Statistics*, pages 1608–1617, 2018.
- [17] Ian Goodfellow, Jean Pouget-Abadie, Mehdi Mirza, Bing Xu, David Warde-Farley, Sherjil Ozair, Aaron Courville, and Yoshua Bengio. Generative adversarial nets. In *Advances in Neural Information Processing Systems*, pages 2672–2680, 2014.
- [18] Ishaan Gulrajani, Faruk Ahmed, Martin Arjovsky, Vincent Dumoulin, and Aaron Courville. Improved training of wasserstein gans. In *Advances in Neural Information Processing Systems*, pages 5767–5777, 2017.
- [19] Martin Heusel, Hubert Ramsauer, Thomas Unterthiner, Bernhard Nessler, and Sepp Hochreiter. Gans trained by a two time-scale update rule converge to a local nash equilibrium. In *Advances in Neural Information Processing Systems*, pages 6626–6637, 2017.
- [20] Phillip Isola, Jun-Yan Zhu, Tinghui Zhou, and Alexei A Efros. Image-to-image translation with conditional adversarial networks. In *Proceedings of the IEEE Conference on Computer Vision and Pattern Recognition*, pages 1125–1134, 2017.
- [21] Michael I Jordan, Jason D Lee, and Yun Yang. Communication-efficient distributed statistical inference. *Journal of the American Statistical Association*, 114(526):668–681, 2019.
- [22] Lili Ju, Qiang Du, and Max Gunzburger. Probabilistic methods for centroidal voronoi tessellations and their parallel implementations. *Parallel Computing*, 28(10):1477–1500, 2002.
- [23] Leonid Vitalevich Kantorovich. On an effective method of solving certain classes of extremal problems. *Dokl. Akad. Nauk. USSR*, 28:212–215, 1940.

- [24] Diederik P Kingma and Max Welling. Auto-encoding variational bayes. *International Conference on Learning Representations*, pages 1–9, 2014.
- [25] Soheil Kolouri, Phillip E Pope, Charles E Martin, and Gustavo K Rohde. Sliced-wasserstein auto-encoders. *International Conference on Learning Representations*, pages 1–13, 2018.
- [26] Soheil Kolouri, Kimia Nadjahi, Umut Simsekli, Roland Badeau, and Gustavo Rohde. Generalized sliced wasserstein distances. *Advances in Neural Information Processing Systems*, pages 261–272, 2019.
- [27] Yann LeCun, Léon Bottou, Yoshua Bengio, Patrick Haffner, et al. Gradient-based learning applied to document recognition. *Proceedings of the IEEE*, 86(11):2278–2324, 1998.
- [28] Na Lei, Dongsheng An, Yang Guo, Kehua Su, Shixia Liu, Zhongxuan Luo, Shing-Tung Yau, and Xianfeng Gu. A geometric understanding of deep learning. *Engineering*, 6(3):361–374, 2020.
- [29] Chris Junchi Li, Lei Li, Junyang Qian, and Jian-Guo Liu. Batch size matters: a diffusion approximation framework on nonconvex stochastic gradient descent. *CoRR abs/1705.07562*, 2017.
- [30] Chun-Liang Li, Wei-Cheng Chang, Yu Cheng, Yiming Yang, and Barnabás Póczos. Mmd gan: towards deeper understanding of moment matching network. *Advances in Neural Information Processing Systems*, pages 2203–2213, 2017.
- [31] Tianyi Lin, Nhat Ho, and Michael I Jordan. On efficient optimal transport: An analysis of greedy and accelerated mirror descent algorithms. *International Conference on Machine Learning*, pages 1–10, 2019.
- [32] Tianyi Lin, Chenyou Fan, Nhat Ho, Marco Cuturi, and Michael I Jordan. Projection robust wasserstein distance and riemannian optimization. *Advances in Neural Information Processing Systems*, pages 1–14, 2020.
- [33] Ziwei Liu, Ping Luo, Xiaogang Wang, and Xiaoou Tang. Deep learning face attributes in the wild. In *Proceedings of the IEEE International Conference on Computer Vision*, pages 3730–3738, 2015.
- [34] Mario Lucic, Karol Kurach, Marcin Michalski, Sylvain Gelly, and Olivier Bousquet. Are gans created equal? a large-scale study. In *Advances in Neural Information Processing Systems*, pages 700–709, 2018.
- [35] James MacQueen. Some methods for classification and analysis of multivariate observations. *Proceedings of the Fifth Berkeley Symposium on Mathematical Statistics and Probability*, 1(14):281–297, 1967.
- [36] Alireza Makhzani, Jonathon Shlens, Navdeep Jaitly, Ian Goodfellow, and Brendan Frey. Adversarial autoencoders. *International Conference on Learning Representations*, pages 1–10, 2016.

- [37] Takeru Miyato, Toshiki Kataoka, Masanori Koyama, and Yuichi Yoshida. Spectral normalization for generative adversarial networks. *International Conference on Learning Representations*, pages 1–12, 2018.
- [38] Khai Nguyen, Nhat Ho, Tung Pham, and Hung Bui. Distributional sliced-wasserstein and applications to generative modeling. *International Conference on Learning Representations*, pages 1–11, 2020.
- [39] Ingram Olkin and Friedrich Pukelsheim. The distance between two random vectors with given dispersion matrices. *Linear Algebra and its Applications*, 48:257–263, 1982.
- [40] François-Pierre Paty and Marco Cuturi. Subspace robust wasserstein distances. *International Conference on Machine Learning*, pages 1–10, 2019.
- [41] Tim Salimans, Ian Goodfellow, Wojciech Zaremba, Vicki Cheung, Alec Radford, and Xi Chen. Improved techniques for training gans. In *Advances in Neural Information Processing Systems*, pages 2234–2242, 2016.
- [42] Max Sommerfeld and Axel Munk. Inference for empirical wasserstein distances on finite spaces. *Journal of the Royal Statistical Society: Series B (Statistical Methodology)*, 80(1):219–238, 2018.
- [43] Ilya Tolstikhin, Olivier Bousquet, Sylvain Gelly, and Bernhard Schoelkopf. Wasserstein auto-encoders. *International Conference on Learning Representations*, pages 1–13, 2017.
- [44] Cédric Villani. *Topics in optimal transportation*. Number 58. American Mathematical Soc., 2003. ISBN 0-8218-3312-X.
- [45] Cédric Villani. *Optimal transport: old and new*, volume 338. Springer Science & Business Media, 2008.
- [46] Jonathan Weed, Francis Bach, et al. Sharp asymptotic and finite-sample rates of convergence of empirical measures in wasserstein distance. *Bernoulli*, 25(4A):2620–2648, 2019.
- [47] Fisher Yu, Ari Seff, Yinda Zhang, Shuran Song, Thomas Funkhouser, and Jianxiong Xiao. Lsun: Construction of a large-scale image dataset using deep learning with humans in the loop. *CoRR abs/1506.03365*, 2015.